Segregation Kinetics of Topologically Modified (DNA-)Polymers in Confinement

A Thesis

submitted to
Indian Institute of Science Education and Research Pune
in partial fulfillment of the requirements for the
BS-MS Dual Degree Programme

by

Harsh Doshi

Indian Institute of Science Education and Research Pune
Dr. Homi Bhabha Road,
Pashan, Pune 411008, INDIA.

March, 2025

Supervisor: Dr Apratim Chatterji

Certificate

This is to certify that this dissertation entitled "Segregation Kinetics of Topologically Modified (DNA-)Polymers in Confinement" towards the partial fulfilment of the BS-MS dual degree programme at the Indian Institute of Science Education and Research, Pune, represents study/work carried out by Harsh Doshi at the Indian Institute of Science Education and Research, Pune, under the supervision of Dr Apratim Chatterji, Professor, Department of Physics, during the academic year 2024-2025.

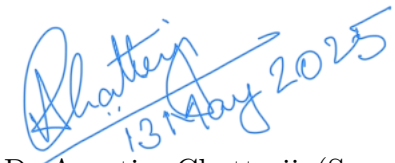

Dr Apratim Chatterji (Supervisor)

Dr Shivprasad Patil (Expert)

Committee:

Dr Apratim Chatterji

Dr Shivprasad Patil

This thesis is dedicated to my family: my parents and my siblings.

Declaration

I hereby declare that the matter embodied in the report entitled "Segregation Kinetics of Topologically Modified (DNA-)Polymers in Confinement" are the results of the work carried out by me at the Department of Physics, Indian Institute of Science Education and Research (IISER) Pune, under the supervision of Dr Apratim Chatterji and the same has not been submitted elsewhere for any other degree. Wherever others contribute, every effort is made to indicate this clearly, with due reference to the literature and acknowledgement of collaborative research and discussions.

Harsh Doshi
Roll No.: 20201187

Acknowledgments

I would like to acknowledge the constant, encouraging, and intellectual support provided by my supervisor, Professor Apratim Chatterji. I could not have accomplished the work in this thesis without his expert guidance and patient motivation. Throughout this project, he has always been approachable and willing to discuss new ideas and the data generated. His excitement and advice have helped me to continue even when I was stuck on some aspect of the project. I would also like to acknowledge the guidance and friendship I found in other members of Professor Chatterji's group. These include the current members (at the time of writing this thesis): Shreerang, Dhruv, Kingkini, Snigdha, Shailesh, Om, Karan, and Rushikesh. They have always been open to discussing new ideas, as well as agreeing to critique my work and the way I communicate it.

I would also like to acknowledge my seniors Sanjay, Vaibhav, and Adrian, who were part of the group when I first joined. I am particularly grateful to Sanjay since he provided guidance when I was first learning about simulating polymers.

I acknowledge using the computing cluster facility assigned to Professor Apratim as well as the PARAM BRAHMA high performance computing facility.

My friends deserve mentions as well. I am grateful to them for listening to my rants about the project and giving helpful advice. These include but are not limited to Mayank, Sumit, Ridham, Prerana, Ayush, and Khakha. Finally, I would like to thank my family, including my parents and my siblings Anand and Khushi, for their constant moral support. Without them, I would not be here at IISER, let alone writing this thesis.

Abstract

It is known that when two self-avoiding polymers are confined in a cylindrical space, they spontaneously evolve towards a state in which the polymers are segregated along the long axis of the cylinder. In such a segregated state, the conformational entropy of both polymers is higher than that of a state where they are mixed. In this computational work, we systematically study the effect of topological modifications to the polymer contour on the segregation speed of these polymers via simulations. The simplest topology we consider is a ring, and we introduce modifications by adding smaller loops to this ring contour. We observe that the speed of the entropic segregation increases with increasing the number of loops of the topology while keeping the total length of the contour constant. The effect of such smaller loops could be relevant for the DNA present in simple bacteria such as E. coli. Additionally, we hope that such topological modifications can be harnessed by synthetic polymers for industrial applications.

Contents

Abstract **xi**

1 Introduction **4**

1.1 Introduction to Soft Matter 4

1.2 History of Soft Matter 5

1.3 Polymer physics 6

1.4 Thesis Outline 14

2 Model and Methods **15**

2.1 Model 15

2.2 Modifying topologies 18

2.3 Initialization and consequent challenges 21

2.4 Validating mixed states of polymers 24

2.5 Finding Segregation Time 29

2.6 Plotting Segregation Times 31

2.7 Statistical Test 32

3 Results **34**

3.1 *Recenter* 34

3.2 *Fixing-Bonding* 40
3.3 *Replication-like* 43
3.4 *Mutual Attraction* 46
3.5 *Recenter*: 500 monomers 49
3.6 *Fixing-Bonding*: 500 monomers 53
3.7 *Replication-like*: 500 monomers 55
3.8 *Mutual Attraction*: 500 monomers 57
3.9 Statistical Tests 59

4 Discussion **62**

List of Figures

1.1 Coarse-grained polymer 7

1.2 Spontaneous segregation of polymers in cylindrical confinement 12

2.1 WCA and FENE potentials 17

2.2 Architecture or topology diagrams 20

2.3 Diagrams of initialization procedures 23

2.4 Sections of the cylinder for calculating monomer density 26

2.5 Polymer orientation diagrams 27

2.6 Segregation trajectory example 30

2.7 Box plot example 31

3.1 Mixed state quantities for Arc0 (200) polymers mixed using the *Recenter* procedure. 35

3.2 Mixed state quantities for Arc-1-10 (200) polymers mixed using the *Recenter* procedure 36

3.3 Pair correlation functions of mixed and segregated states 38

3.4 Segregation data for the *Recenter* procedure (200 monomers) 39

3.5 Mixed state quantities for Arc-1-10 (200) polymers mixed using the *Fixing-Bonding* procedure 41

3.6 Segregation data for the *Fixing-Bonding* procedure (200 monomers) 43

3.7 Mixed state quantities for Arc-1-10 (200) polymers mixed using the *Replication-like* procedure 44

3.8 Segregation data for the *Replication-like* procedure (200 monomers) 45

3.9 Mixed state quantities for Arc-1-10 (200) polymers mixed using the *Mutual Attraction* procedure 46

3.10 Segregation data for the *Mutual Attraction* procedure (200 monomers) 48

3.11 Polymers showing threading 49

3.12 Mixed state quantities for Arc-1-10 (500) polymers mixed using the *Recenter* procedure 50

3.13 Segregation data for the *Recenter* procedure (500 monomers) 51

3.14 Segregation time comparison for different orientations 52

3.15 Mixed state quantities for Arc-1-10 (500) polymers mixed using the *Fixing-Bonding* procedure 54

3.16 Segregation data for the *Fixing-Bonding* procedure (500 monomers) 55

3.17 Mixed state quantities for Arc-1-10 (500) polymers mixed using the *Replication-like* procedure 56

3.18 Segregation data for the *Replication-like* procedure (500 monomers) 57

3.19 Mixed state quantities for Arc-1-10 (500) polymers mixed using the *Mutual Attraction* procedure 58

3.20 Segregation data for the *Mutual Attraction* procedure (500 monomers) 59

4.1 Energy time series of a segregation run 63

List of Tables

3.1 Table of *p-values* for comparisons between architectures using the *Recenter* (200) procedure. 60

3.2 Table of *p-values* for comparisons between architectures using the *Recenter* (500) procedure. 60

Chapter 1

Introduction

1.1 Introduction to Soft Matter

What is "soft matter"? Soft matter constitutes various classes of materials, all of which share a common property: they are "soft". By soft, we mean that the materials can be deformed easily, even by applying weak forces. Often, the mechanical properties of soft matter fall in an intermediate regime between liquids and solids. Hence, these materials are also called "complex fluids". Examples of soft matter include foams, gels, polymer solutions, and liquid crystals, among others. Even biological matter such as tissue and cells are considered under this classification. Despite the major differences in the above classes of materials, they share common properties which allow them to be studied under the universal framework of "soft matter physics" [1–5].

Soft materials are built by units that have an intermediate or 'mesoscopic' size scale. The units are much bigger than individual atoms, though much smaller than the macroscopic objects humans are used to. Since the building blocks are much bigger than atoms, the behaviour of such materials is not influenced by quantum effects. However, they are small enough to be strongly affected by the thermal fluctuations of their surroundings. In addition, the interactions between different units are weaker than interactions in hard, crystalline solids. They are of the order of the thermal energy in the system, which is another reason why thermal effects play an important role in these materials. The mesoscopic size of units and their weak interactions are responsible for the soft nature of such materials [1, 2, 5].

Soft matter materials often show interesting properties because of the way large collections of these building blocks interact together. These building blocks tend to form higher-order structures via a process called 'self-assembly', which is the mechanism behind the action of soaps and the formation of biological protein complexes. A consequence of the collective nature of these materials is that their relaxation times are slow. If a material is perturbed under some transient external force, it can take a long time to return to its equilibrium state. Thus, many soft matter materials exhibit interesting non-equilibrium properties [2, 4].

These materials are often studied under the framework of statistical mechanics and non-equilibrium physics. In any closed system at constant temperature having constant volume, at equilibrium, the Helmholtz free energy F is minimized.

$$F = U - TS \tag{1.1}$$

where U is the interaction energy in the system, T is the temperature, and S is the entropy of the system. As discussed, the interaction energies in soft matter systems are comparable to the thermal energy. Thus, the energy term and the entropic term both contribute, and their interplay gives interesting properties to soft matter systems [1, 2, 5]. For example, the entropic term plays a pivotal role in a system of polymers that are kept in a small box. This leads to a peculiar property that this thesis is based on.

Soft materials are extensively used in consumer products, such as gels, soaps, plastics, etc. Thus, it is justified to study these materials to gain a better understanding of their properties and applications. In recent decades, the framework of studying soft matter has been extended to study biological systems in terms of a physical description. Such a framework has the potential to illuminate mechanistic processes in biology that have remained elusive and, thus, deepen our understanding of the natural world.

1.2 History of Soft Matter

Perhaps the most fundamental discovery that contributed to the development of soft matter physics was Brownian motion. In 1827, Robert Brown observed the random motion of pollen grains in water [5]. Almost a century passed before Albert Einstein and Marian

Smoluchowski independently explained the random motion due to thermal agitation of the surrounding medium [2]. This was one of the successes of statistical mechanics.

By this time in the early 20th century, many interesting and unconventional materials had gained popularity. Liquid crystals were discovered by Friedrich Reinitzer in 1888 and later characterized by Otto Lehmann [5]. In 1920, the idea of polymers as macromolecules was pioneered by Hermann Staudinger, though polymers already existed and were being used by that time [5, 6]. In the late 19th century, Thomas Graham provided convincing evidence that matter could exist as fine granular particles and called them "colloids" [7].

These three separate fields were developed independently, among developments in other materials as well. It was only in the late 20th century that people began realising that all these interesting properties could be explained in a unified framework. In particular, the work of Sam Edwards and Pierre-Gilles de Gennes [2] on liquid crystals and polymers led to this framework, which came to be known as soft matter physics. The 1991 Nobel Prize in Physics was awarded to de Gennes for his contributions.

In recent years, the field of soft matter physics has continued to develop at a brisk pace. This has been driven by improvements in instrumentation and microscopy used to probe these soft matter materials. The increase in computational power has facilitated sophisticated simulations and numerical techniques, contributing to our understanding of the structure and dynamics of soft matter. Newer materials with more complex properties have also been developed, one of which is active matter materials, where particles actively consume energy to influence the material behaviour. These principles have also been extremely useful in studying biological systems, which are made of soft and living (active) matter [8, 9].

1.3 Polymer physics

The work done in this thesis is based on a special property of polymers. When two polymers are placed in cylindrical confinement, they spontaneously segregate. In order to understand this property, this chapter briefly summarises the preliminaries of polymer physics required.

1.3.1 What are polymers?

Polymers are large molecules that consist of many repeating units called 'monomers'. They are made by linking many smaller monomer molecules together to form a big structure. Polymer physics is a subfield of soft matter physics that describes the structural and dynamic properties of such polymers. It takes a very general approach: it uses a framework that is applicable to a wide variety of polymers, irrespective of their chemical composition. Usually, a coarse-grained approach is taken, where multiple chemical units are grouped together in a single body (see Figure 1.1) [10]. This single body is taken to be a monomer, and its internal structure is ignored.

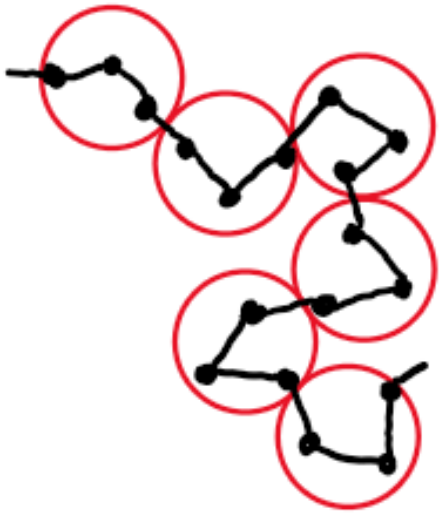

Figure 1.1: A cartoon representation of the coarse-graining of a polymer. The black beads represent chemical units connected by bonds (black lines). A group of three such units is grouped into a single coarse-grained monomer represented by the red circle. The black bead polymer can be replaced by the coarse-grained red-circle polymer.

Polymers can exist in a large number of different possible conformations or structures. These conformations are influenced by the interactions between different monomers and with the environment. This interplay between the interactions and structure manifests as fascinating properties, one of which is the basis for this thesis. In this thesis, we consider the polymers to be in a solvent at a finite temperature. The thermal motion of the solvent molecules results in the incessant motion of the monomers as well. As a result, the polymer keeps changing its conformation when suspended in a solvent. The different conformations that a polymer can take are described within the framework of statistical mechanics.

This can be motivated by the following example. Consider a linear polymer that consists of N monomers connected sequentially. Each conformation of this polymer can be mapped to a realisation of a three-dimensional random walk with N steps [10]. This mapping is very useful to calculate and predict the properties of the polymer. More details are provided in the following subsection.

The power of statistical mechanics can be used to derive 'scaling relations' that describe the properties of polymers. Usually, these relations give information about how a polymer property changes with a change in the length of the polymer or N. Taking the same example as before, a scaling relation involving the size of a linear polymer would look like:

$$R \propto N^{\alpha} \tag{1.2}$$

where R is a measure of the size of the polymer, N is the length, and α is a real number constant that describes the power law relation between R and N. Such a relation is useful since it can describe the polymer at multiple scales and levels of coarse-graining.

1.3.2 Size of polymers

A polymer can take many conformations, with a defined arrangement of N monomers in each of them. We can define the size of a polymer as the end-to-end vector $\mathbf{R}_{ee}$ which is given by:

$$\mathbf{R}_{ee} = \mathbf{r}_N - \mathbf{r}_1 = \sum_{i=1}^{N-1} \mathbf{b}_i \tag{1.3}$$

where $\mathbf{r}_i$ is the position vector of the ith monomer, and $\mathbf{b}_i$ is the bond vector defined by $\mathbf{b}_i = \mathbf{r}_{i+1} - \mathbf{r}_i$. Since the conformation of the polymer is constantly changing, we consider an average value of such a quantity to represent the size of the polymer.

First, we consider the simplest case of an 'ideal' polymer or chain. In this case, the non-bonded monomers do not interact with each other and can pass through one another. We can calculate the average size of such a polymer using the random walk analogy. The bond vectors $\mathbf{b}_i$ are taken as random steps of a fixed length in a random walk of N steps, where each bond can point in any random direction. Using properties of random walks, we get $\langle \mathbf{R}_{ee} \rangle = 0$ since the end-to-end vector can point in any direction and will cancel out

on taking an average over all conformations in the statistical ensemble. Instead, we can calculate $\langle \mathbf{R}_{ee}^2 \rangle$ to get a non-zero value. Again, via the random walk analogy, we get [10],

$$\langle \mathbf{R}_{ee}^2 \rangle = b^2 N \tag{1.4}$$

where $b = |\mathbf{b}_i|$ is the equilibrium bond length.

This quantity is useful for linear polymers, but it can be ambiguous when defined for other forms of polymers, such as branched or ring polymers. A more useful quantity is the radius of gyration R_g given by,

$$R_g^2 = \sum_{i=1}^{N} (\mathbf{r}_i - \mathbf{r}_{com})^2; \quad \text{where} \quad \mathbf{r}_{com} = \sum_{i=1}^{N} \mathbf{r}_i \tag{1.5}$$

Here, $\mathbf{r}_{com}$ is the position for the centre of mass (CoM) of the polymer.

The random walk analogy can be used to obtain [10]

$$R_g = \frac{bN^{0.5}}{\sqrt{6}} \tag{1.6}$$

for ideal linear polymers.

In reality, polymers are not ideal, and their monomers interact with one another. A simple case of real polymers is when the non-bonded monomer interaction is a short-range repulsive potential that prevents two monomers from overlapping. In this case, the polymer is described by a 'self-avoiding' random walk, which changes the above simple relation to [11]

$$R_{g,l} = \frac{bN^{\nu}}{\sqrt{(1+2\nu)(2+2\nu)}} \tag{1.7}$$

where $R_{g,l}$ is the radius of gyration of a real linear polymer and ν is the scaling exponent which has its value close to 3/5 or 0.6 [10]. In this thesis, the basic polymer architecture we consider is a ring, and its radius of gyration $R_{g,r}$ is given by [11],

$$R_{g,r} = \sqrt{f} R_{g,l} \tag{1.8}$$

where f is a numerical prefactor equal to the ratio of the radii of gyration of ring and linear polymers. We have taken $f = 0.55$ [11].

Note that in all cases above, the analysis assumes that the solvent is a 'good solvent' or an 'athermal solvent' [10]. A good solvent means that the monomer-solvent interaction is more favourable than the monomer-monomer interaction. As a result, the polymer tends to spread itself out inside the solvent. An athermal solvent is the case when only the repulsive monomer-monomer interactions are relevant, which occurs at high temperatures. Again, in this case, the polymer spreads itself out to avoid monomer-monomer overlaps.

One should also note that these estimates for sizes are valid when the polymers are in a dilute solution. Two different polymers do not interact with one another since they are very far apart in space. As the concentration increases, the polymers come closer and closer till different polymers start touching each other. The polymers may not be able to occupy the same volume as earlier, leading to a reduction in size. Such a condition is called a 'semi-dilute' solution. The work done in this thesis deals mainly with polymers in this regime.

1.3.3 Polymer Dynamics

The motion of polymers is due to the collective motion of the monomers driven by the thermal agitation of the solvent particles. Due to this, the polymer motion is random, just as the motion of the monomers is. We can calculate the characteristic time of diffusion of the entire polymer by calculating the mean square displacement of its centre of mass. The dependence of the polymer's motion on its size can be predicted theoretically.

Here, we use the Rouse model of polymer dynamics. It assumes a 'free-draining' solvent such that the solvent molecules are not dragged along by the polymer as it diffuses. So, the drag/friction felt by the polymer is simply the sum of the contributions from each monomer.

This model predicts the time it takes for the polymer to move a distance equal to its own size is τ_R given by [10],

$$\tau_R \approx \tau_0 N^{1+2\nu} \tag{1.9}$$

where τ_R is called the Rouse time, τ_0 is the time taken by a single free monomer to diffuse its own size, N is the number of monomers in the polymer, and ν is the scaling exponent that gives the size (radius of gyration R_g) as a power law of N. The time τ_R is also called the relaxation time and refers to a characteristic timescale over which the polymer changes

its conformation substantially.

For ideal polymers, $\nu = 0.5$, thus, $\tau_R \approx \tau_0 N^2$. These expressions are valid for an ideal polymer in a dilute solution. Additionally, the freely-draining assumption ignores any hydrodynamic effects that are present in real solutions. However, the work in this thesis only involves simulations without modelling hydrodynamics effects; thus, the use of Rouse times is justified.

1.3.4 Topological modifications to polymers

In recent times, there has been an increased interest in ring polymers and additional topological modifications made to the ring [12]. Ring polymers have interested physicists since they do not have ends like a linear polymer and, thus, show different dynamics properties[13]. More recently, people have also realised the applicability of polymer physics to chromosomes [14]. Bacterial chromosomes, in particular, are circular, making them a naturally occurring ring polymer system.

People have also been interested in studying topological features like loops and knots in these polymers [15]. In a linear polymer, such knots can be unravelled by moving one end of the polymer in a particular way. However, when such a knot exists on a ring polymer, it can be resolved without breaking the polymer bonds. Such structures present in chromosomes can alter the function of cellular processes.

In this thesis, we consider loops or subloops formed on the polymer by connecting specific points of its contour (explained in more detail in Section 2.2). This is motivated by naturally occurring looped structures on chromosomes in biological cells. Many proteins have been found that can form such looped structures of DNA to facilitate a function [16, 17]. Although these loops are dynamic, we model them as fixed and permanent. Our aim is to build an understanding of the fundamental properties introduced by these loops, and hence, we consider the simpler case where the loops are static.

Work has been done on such systems taken in confinement [18, 19] showing that loops can lead to spatial organization of different segments. There have also been studies investigating the role of such loops in the process of chromosome segregation in bacterial cells [20, 21]. This thesis aims to extend our understanding of topological modifications in the context of

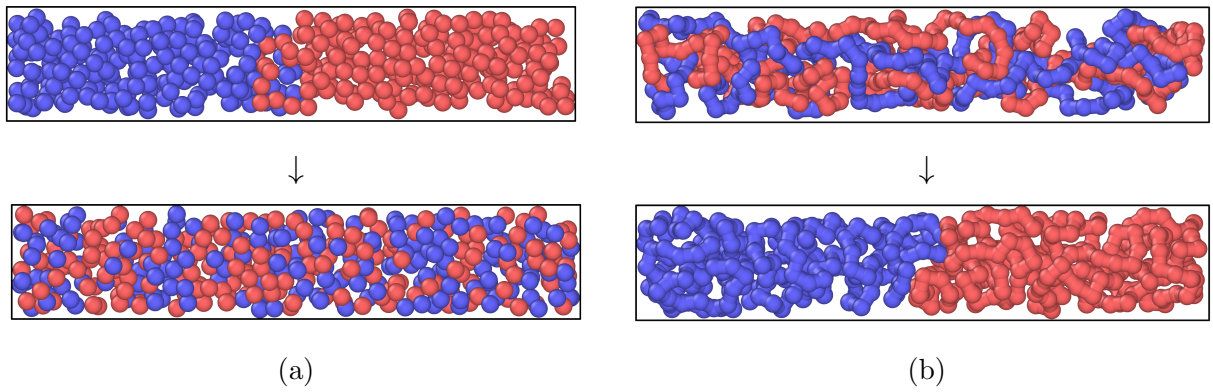

Figure 1.2: Snapshots of a system of (a) gas molecules and (b) ring polymers in cylindrical confinement. In (a), the red and blue colours represent molecules originating from a particular side of the cylinder. As the gas system evolves, the molecules mix together. In (b), the red and blue colours represent monomers belonging to the two different polymers. In the polymer system, the polymers segregate spontaneously from a mixed state.

segregation.

1.3.5 Segregation of Polymers

In a semi-dilute solution, two polymers can come close to each other and interpenetrate each other's volumes. When they are in such a state, we call the two polymers overlapped or 'mixed'. It has been shown that the free energy of such a state of two linear polymers is of the order of thermal energy [22]. Thus, such mixed states are frequently attained in solution.

However, the situation is quite different when the polymers are confined in a small cylinder. Under the right conditions of confinement, the free energy of mixing can be very high for two polymers. In such cases, the polymers prefer to stay 'segregated' as opposed to mixed [23–25]. This phenomenon seems quite counter-intuitive as it is the exact opposite effect of two separated gases mixing in a box (see Figure 1.2). In a gas, the entropy of mixing is higher, thus, entropy is maximized on mixing. Similarly, the segregation of polymers is driven by an increase in entropy, as explained in brief below.

For two polymers in a mixed state in cylindrical confinement, the number of conformations Ω_{mix} they can take is reduced. Instead, if the polymers are segregated, they can access

a higher number of conformations Ω_{seg} collectively [26]. By virtue of Boltzmann entropy $S = k_B \log\Omega$, the entropy increases in going from the mixed to the segregated state.

This free energy difference between mixed and segregated can be quantified by the blob-theory scaling approach [10, 26]. In this theoretical approach, each polymer is divided into multiple blobs with a characteristic length scale. Within this length scale of a single blob, the polymer behaves as if it is unperturbed by the confinement imposed. Beyond this, the polymer statistics deviate from those of the dilute case. Thus, beyond this blob length, the polymer pays a free energy cost due to the effect of the perturbation. This free energy cost is taken of the order of k_BT per blob. The more blobs there are in the entire system, the higher the free energy of the system.

In the case of two polymers confined in a cylinder, the polymers can be arranged in a linear array of blobs. However, when they are mixed or overlapped, the effective confinement felt by each polymer increases, as does the number of blobs. Thus, the free energy of a segregated state is lower than that of a mixed state. A more detailed and quantitative calculation is done in the appendix of [18].

This tendency of segregation has been used in a biological context to explain the segregation of bacterial chromosomes [26]. There have been many studies in recent times investigating this segregation property of polymers in spherical confinement [19, 27], in cylindrical confinement with crowders [28], and by modifying topology [18, 26, 29, 30].

This thesis focuses on the tendency of polymers to segregate in cylindrical confinement when their topologies or architectures are modified. Certain proteins are known to form loops on chromosomes [16]. Motivated by such biological structures, we introduce static loops on a ring polymer and study how their segregation speeds change. A very similar study has been performed before [18], but it considered polymers that can undergo chain crossing, which is relevant to biology. In this thesis, we use simulations to study 'dead' synthetic polymers whose chains cannot cross. Additionally, we systematically modify the topology of polymers to obtain a fundamental understanding of the link between topology and segregation. The hope is that this work will not only be useful in biological contexts of chromosome segregation but can also be used to design industrial applications.

1.4 Thesis Outline

In this thesis, we use simulations to study the time of segregation of two polymers confined in a cylinder. Ideally, one should include hydrodynamics effects in simulations for a model closer to reality, but we ignore such effects throughout this work. Here, our aim is to understand how adding loops to a polymer affects the time taken for segregation. Hydrodynamic effects might drastically affect the time scale on which this process operates, but we do not expect them to change the relative propensity of a topology to segregate.

We start by describing the details of our simulations, how we initialize our system of polymers, and how we measure segregation times in Chapter 2. In Chapter 3, we present our obtained segregation times for the different initialization procedures we use. Finally, we end with Chapter 4, where we discuss the significance of our results.

Chapter 2

Model and Methods

In order to investigate the segregation properties of polymers with modified topologies, we make use of polymer simulations. This chapter explains how the simulations are set up and run and how the data extracted from these simulations are analyzed. For this work, I have followed a common procedure for all simulations. I start with a system of two polymers, both with a specific topology. I run a preliminary simulation to obtain a mixed state of the polymers in confinement. Then, I take the mixed state and run another simulation to observe the segregation of the two polymers (The reason for performing these procedures in separate simulations will be evident later). In the following sections, I give the details of the simulations that I perform and the quantities I calculate to study the system.

2.1 Model

In this work, we perform molecular dynamics (MD) simulations of two non-concatenated coarse-grained polymers confined in a cylindrical geometry. We model the polymers as a chain of monomers connected via springs or bonds (Kremer-Grest model [31]). Each monomer in our simulations might correspond to many chemical monomers of an actual polymer. We do not simulate each and every chemical monomer or atom of the polymer. Instead, we simulate a cluster of such atoms as a single body, and we expect that the physics at large scales will be unaffected [10].

Each monomer can interact in two ways with other monomers. Consecutive or bonded monomers are held together by a bonding potential. On top of this, all monomers interact via a short-ranged, purely repulsive potential to avoid overlap.

The repulsive interaction is given by the Weeks-Chandler-Anderson (WCA) potential [32],

$$U_{WCA}(r) = \begin{cases} 4\epsilon \left[\left(\frac{\sigma}{r}\right)^{12} - \left(\frac{\sigma}{r}\right)^{6} \right] + \epsilon & ; r < r_0 \\ 0 & ; r > r_0 \end{cases} \tag{2.1}$$

where r is the distance between the interacting monomers, σ is the monomer diameter, and ϵ is the energy scale in our simulations. $r_0 = 2^{\frac{1}{6}}\sigma$ is the cutoff distance beyond which the potential is zero. This potential acts at very short ranges when the monomer centres are closer than the cutoff distance. At the cutoff, the potential continuously goes to 0. Such shape of the potential ensures that monomers which come close to each other feel a repulsion and move apart. Monomers with a separation beyond the cutoff are unaffected. We set the units by defining $\sigma = 1$ and $\epsilon = 1$ in our simulations.

The particles interact with the cylindrical confining surface (or wall) via the same WCA potential form. A key difference is that the length scale for this wall potential is $\sigma_w = \sigma/2$, half of the potential between monomers. This ensures that the monomer roughly starts feeling the repulsion when its centre is within one radius of the walls.

The bonded monomers interact via the FENE[31] potential, given by

$$U_{FENE}(r) = -\frac{1}{2} K {R_0}^2 \ln \left[1 - \left(\frac{r}{R_0} \right)^2 \right] + U_{WCA}(r) \tag{2.2}$$

where r is the bond length, K is the spring constant, and R_0 is the maximum extension allowed for the bond. For all simulations, we set $K = 30\,\epsilon/\sigma^2$ and $R_0 = 1.5\,\sigma$. The $U_{WCA}(r)$ term ensures that even bonded monomers cannot overlap with each other.

The simulations are performed in a cylinder of fixed volume with a Langevin thermostat that keeps the temperature fixed. We use the LAMMPS [33] (16 March 2018 version) software package. Each monomer is subject to forces given by the Langevin equation, $m\ddot{\mathbf{r}} = -\nabla U - \xi\dot{\mathbf{r}} + \mathbf{F}_R$ where m is the mass of the monomer, $\mathbf{r}$ is its position, U is the potential acting on the monomer, ξ is the drag coefficient, and $\mathbf{F}_R$ is the random force satisfying the fluctuation-dissipation theorem. The random force represents the collisions of the monomers

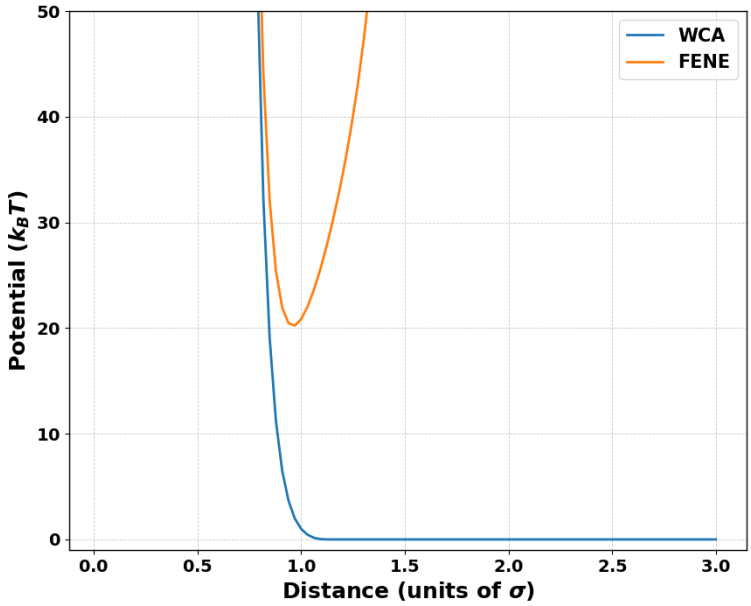

Figure 2.1: The interaction between monomers used in the model of the polymer. The WCA potential exists between all non-bonded monomers to prevent overlap of monomers and between monomers and walls to impose confinement. The FENE bond potential exists between bonded monomers.

with the solvent particles and has the following properties. The individual components come from a Gaussian distribution centred at zero and are uncorrelated with each other. They are uncorrelated in time as well. Thus,

$$\langle \mathbf{F}_R(t) \rangle = 0 \ \forall \, t, \text{ and} \tag{2.3}$$

$$\langle \mathbf{F}_R(t) \cdot \mathbf{F}_R(t') \rangle = \ 2\xi k_B T \ \delta(t - t') \tag{2.4}$$

The latter equation is the fluctuation-dissipation theorem and fixes the magnitude of the random force such that its effect is balanced by the dissipation caused by the drag term. This balance ensures the temperature of the system stays roughly constant. Also, note that the random forces are delta-correlated in time.

The corresponding timescale in our system is defined as $\tau_0 = \sqrt{\frac{m\sigma^2}{\epsilon}}$. The Boltzmann constant k_B and the temperature T are set to 1 so that $k_BT = 1 = \epsilon$. We choose $m = 1$ and $\xi = 1 \, m/\tau_0$ for all monomers.

The equation of motion is integrated using the velocity Verlet algorithm with a time step of $\Delta t = 0.005\tau_0$ for the initialization simulations and $\Delta t = 0.01\tau_0$ for the segregation simulations.

2.2 Modifying topologies

In this section, we define the different topologies or polymer "architectures" we use in this work to study segregation times. Throughout this work, we use 'topology' and 'architecture' interchangeably. The simplest topology we consider is the linear polymer. In our simulations, the monomers in the polymer are indexed from 1 to N, where N is the number of monomers present in the polymer. If the 1st and Nth monomers are bonded together, a ring polymer is formed. This ring polymer is the basis for the more complicated architectures we define below. We introduce additional bonds or "cross-links" between two monomers that are distant along the ring contour to form loops. A diagrammatic representation of different architectures in given in Figure 2.2.

(i) Single-looped architectures: A single cross-link is introduced to the ring polymer. This results in the formation of two subloops in the polymer architecture (see Figure 2.2b). We call these architectures "rotated-8" architectures since they resemble the number '8' rotated by 90 degrees. Depending on where the cross-link is placed, the relative sizes of the two subloops can be varied. We consider multiple architectures by systematically varying the size of the subloops. Such topologies are named in the following way: "ArcR8-3-7 (N)", where ArcR8 represents the rotated-8 architecture. The two integers following ArcR8 (separated by dashes) give the ratio of the sizes of the two loops in the architecture. For example, in a polymer ring of $N = 200$, if we introduce a cross-link between monomers numbered 20 and 80, then one smaller loop (20-80) and one bigger loop (81-200-19) are formed. The sizes of these loops in terms of the number of monomers in them are 60 and 140, respectively. Thus, the ratio of their sizes is 3:7, as is indicated in the name ArcR8-**3-7**. The N following the name indicates the total number of monomers in the polymer, and thus, the complete name of the architecture in the above example is "ArcR8-3-7 (200)".

(ii) Multiple-looped architectures: We introduce a higher number of cross-links to the ring polymer to make more subloops. These cross-links are imposed such that the subloops formed are next to each other along the polymer contour (see Figures 2.2c, 2.2d, and 2.2e).

Again, we systematically increase the number of cross-links to make new architectures. The architecture then consists of a big subloop and a few smaller subloops of equal size clustered together in space. The cross-links are made such that the size of the bigger subloop remains constant across all such architectures, irrespective of the number of smaller subloops. Such topologies are named as "Arc-1-5 (N)". The two integers separated by dashes in the name represent the number of subloops of each kind: big or small. We have only considered one big subloop in this work, so the first integer is 1. The second integer corresponds to the number of cross-links imposed on the ring and, consequently, the number of smaller subloops. Again, N is the number of monomers in the entire polymer.

(iii) Interpolymer cross-links: In some cases, we introduce cross-links between monomers of two different polymers for initialization purposes, as described in the next section, Section 2.3. Such cross-links are made between "corresponding" monomers. These monomers have the same index label along their polymer contour; for example, the ith monomer of a polymer is bonded to the ith monomer of another polymer, which is a cross-link between corresponding monomers.

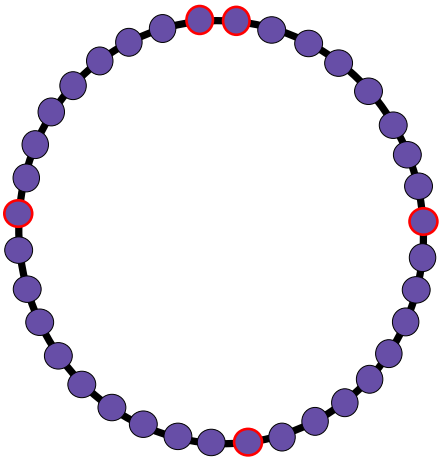

(a) Ring or Arc0 topology

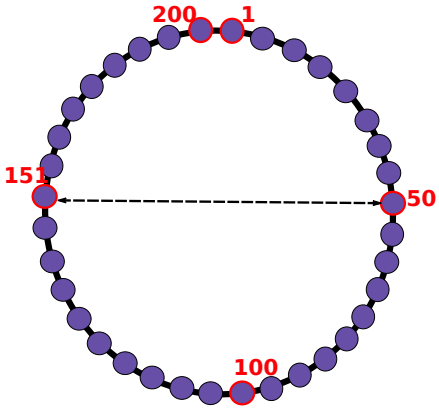

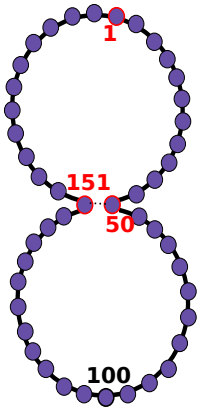

(b) *Single-Looped topology* (Arc-1-1)

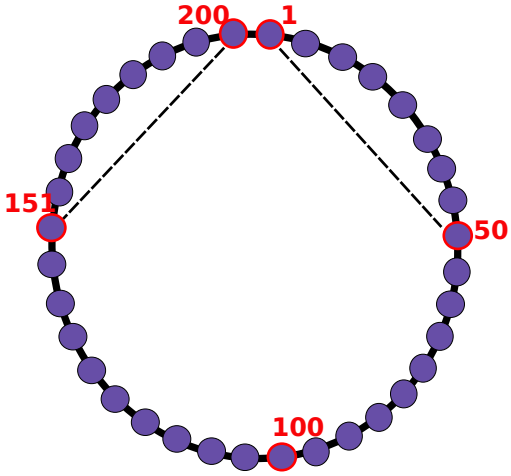

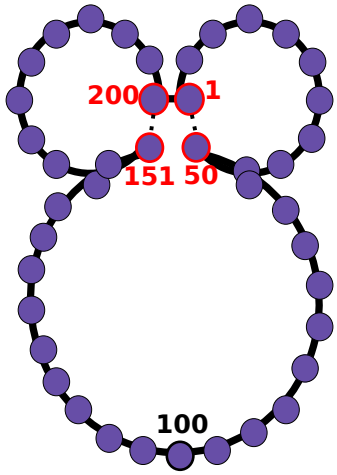

(c) Arc-1-2

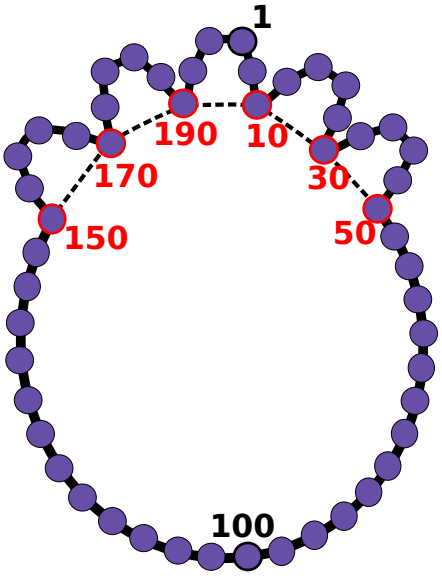

(d) Arc-1-5

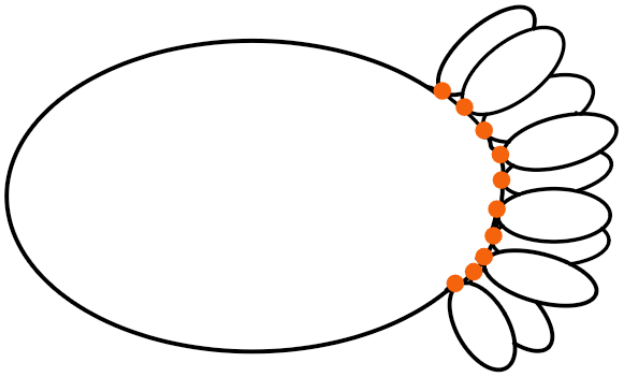

(e) Arc-1-10

Figure 2.2: Schematic diagrams of topologies constructed from individual beads (lavender disks) connected via bonds (black lines) for polymers with 200 monomers. Dashed lines indicate cross-links between two specific monomers. Some of the monomers are labelled with their indices in red and black. In (e), for clarity, the Arc-1-10 diagram is shown as a line diagram instead of explicitly showing the monomers as lavender disks. In the line diagram, the black lines represent the polymer contour, and the orange dots represent cross-links. Credit for a few diagrams: Kingkini Roychoudhury [19]

2.3 Initialization and consequent challenges

A major challenge in studying segregation times is to prepare an initial state of polymers under confinement. This initial state must be such that the polymers are overlapped or "mixed" as opposed to already being segregated into different halves of the confinement. In this study, we consider two polymers "mixed" if their individual centres of mass are sufficiently close to one another along the long axis of the cylinder. When this state starts segregating, the centres of mass move away from each other along the long axis till the two polymers occupy different halves of the cylinder. When working with closed topologies, we start with non-concatenated polymers. This constraint makes the initialization procedure difficult. We wanted a procedure that could robustly generate random initial mixed states that conform to the above constraints. Our goal was to generate multiple mixed states so that we could study segregation from each state via multiple independent simulations. We cannot simply initialize the monomers randomly within the confinement, as that could lead to undesirable concatenations. Thus, we must start with a state with non-concatenated polymers and bring them to mix under confinement.

We came up with several different ways to achieve such a mixing, but not all procedures worked. The procedure we ended up using is a little complicated, but it avoids any of the pitfalls of our failed attempts.

- We start with two polymers that are spatially separated and non-concatenated in a big cylinder ($R >> R_g, L >> R_g$).
- Then, we perform a short off-lattice Monte Carlo simulation to allow the bonds and cross-links between monomers to relax.
- Then, the cylinder is gradually shrunk to obtain the desired confinement while maintaining the topological constraint of non-concatenation.
- Finally, we simulate the polymers in the shrunk cylinder for sufficiently long so that they attain a relaxed state within the confined space.

As discussed previously, the polymers under confinement have higher conformational entropy when they are segregated than when they are mixed. Thus, they have a natural tendency

to evolve to a segregated state. This entropic force is precisely what hinders two non-concatenated polymers in confinement from staying mixed together. If we let this entropic force go unchecked, the polymers would be segregated already by the time the cylinder reaches the desired size after shrinking. There would not be a precise time to say when the segregation started occurring. This would make reliable measurement of segregation time difficult.

To overcome this problem, we introduce additional constraints on the polymers to force the polymers to remain mixed. The constraints are designed such that the polymers are allowed to explore multiple conformations but still remain unsegregated. Once the cylinder size has shrunk down and the polymers have relaxed, we can "switch off" the constraints. As soon as the constraints stop acting, the entropic forces drive the segregation of the polymers. Since we control when to switch off the constraints, we can precisely measure when the segregation started occurring and, thus, reliably measure the time taken for segregation. We used four different constraints to achieve mixed states of polymers:

(i) "*Recenter*" *or "Fixed centre"*: The centres of mass of the two polymers are constrained to lie in the $z = 0$ plane (or equatorial plane) passing through the centre of the cylinder and perpendicular to the long axis. Figure 2.3a shows this procedure in a rough diagram. In each simulation step of the Langevin dynamics simulation, the monomers move randomly, and thus, the centres of mass of the polymers may not remain fixed. After each step, the positions of all monomers are shifted by the same amount such that the centres of mass of the polymer are brought back to the original position without changing the conformation of the polymer. This constraint prevents the polymers' centres of mass from moving apart and keeps them overlapped.

(ii) "*Fixing-Bonding*": From each polymer, we fix two diametrically opposite monomers on the contour in place; the positions of these monomers are fixed at points close to the centre of the cylinder and do not change with time. These monomers are fixed on the equatorial plane ($z = 0$ plane) of the cylinder at a distance of $R/2$ from the cylinder axis, where R is the radius of the cylinder. In addition, we introduce extra bonds connecting a monomer with the corresponding monomer from the other polymer. Two such bonds are introduced between diametrically opposite monomers that are far away from fixed monomers (see Figure 2.3b). The bond is modelled as a harmonic potential $U_{harm} = \frac{1}{2}\kappa(r - r_0)^2$; where the spring constant $\kappa = 1000\,\epsilon/\sigma^2$ and the equilibrium bond distance $r_0 = 1\,\sigma$.

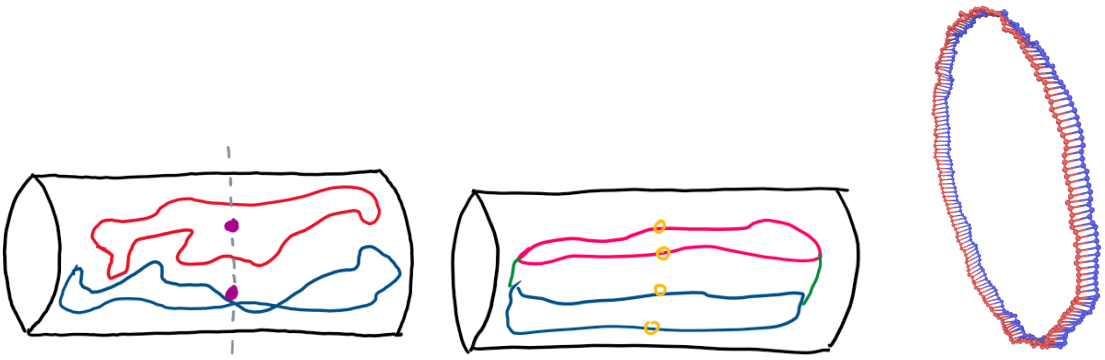

(a) (b) (c)

Figure 2.3: Schematic diagrams showing three of the constraints imposed during the initialization of the polymers in a mixed state. (a) *Recenter*: The centres of mass (purple dots) of the two polymers are kept fixed in the equatorial plane. (b) *Fixing-Bonding*: Two monomers from each polymer are kept fixed in space (yellow circles), and the monomers close to the poles are bonded via interpolymer bonds (green lines). (c) *Replication-like*: Each and every monomer is bonded to the corresponding monomer of the other polymer via interpolymer bonds.

(iii) "*Replication-like*": Each monomer of a polymer is bonded to the corresponding monomer from the other polymer via a weak harmonic potential with the form given in *(ii) "Fixing-Bonding"* (see Figure 2.3c). The spring constant κ is chosen as $10\,\epsilon/\sigma^2$, and the equilibrium bond distance r_0 is chosen as 3σ. This set of constraints is termed as *"Replication-like"* since it is similar to how replication of a coarse-grained chromosome is modelled in a previous study [20].

(iv) "*Mutual Attraction*": A weak attractive potential is introduced between monomers belonging to different polymers. Self-polymer interactions continue to be purely repulsive. The attractive potential is given by the LJ potential: $U_{LJ} = 4\epsilon_{LJ}\left[\left(\frac{\sigma_{LJ}}{r}\right)^{12} - \left(\frac{\sigma_{LJ}}{r}\right)^{6}\right] + U_0 \quad ; r < r_0$ and $U_{LJ} = 0; r \geq r_0$. Here, we choose $\epsilon_{LJ} = 0.5\epsilon$, $\sigma_{LJ} = \sigma$, and the cutoff distance $r_0 = 2.5\sigma$. U_0 is an additive constant such that U_{LJ} smoothly goes to zero at $r = r_0$.

We run simulations using one of these procedures at a time while performing the steps outlined to shrink the cylinder and relax the polymers. The last snapshot of the simulation is taken as an initial mixed state for the subsequent segregation simulation. We calculate and plot a few quantities to ensure the validity of the mixed state. More details regarding these quantities can be found in Section 2.4.

Once the mixed states have been validated, we can use the obtained mixed state to study the time of segregation for that topology.

2.4 Validating mixed states of polymers

As described in the previous section (Section 2.3), we start by running a simulation to create a mixed state of two polymers. We can then use this mixed state as a starting point for the segregation simulations.

To remind the reader, we perform the initialization in two parts. First, we shrink a big cylinder with relaxed polymers till the desired confinement is achieved. This procedure avoids unwanted concatenations between polymers. Second, we impose additional constraints on the system that prevents the polymers from evolving to an equilibrium segregated state. Both these procedures could introduce unintentional artefacts in our mixed states. It is not practical to look at the movies (visualizations of the simulations) for each and every independent run to find out whether any artefacts are present. Thus, we plot a few representative quantities that allow us to study the system during this initialization simulation and observe anomalies if present. Note that the data for these quantities is collected only after the cylinder is shrunk down to the desired dimensions.

2.4.1 Monomer densities

The most common quantity that we use to study the system is "monomer density". It is the probability density curve that gives the probability of finding any monomer in a particular section of the cylinder over the length of the entire simulation. We plot many variations of this quantity that allow us to study the spatial localization of monomers along various dimensions of the cylinder.

(i) Total Monomer Density:

We plot the probability density of finding any monomer at a particular position along the long axis of the cylinder. We divide the cylinder into thin disk-like volumes and find the probability of finding any monomer in a particular disk over the length of the entire

simulation. The thin disks are of finite width, and we consider them bins for the density curve. Essentially, this is a probability density plotted along the long axis or z-axis, and is given by

$$P(z) = \frac{n(z)}{n_{total}\Delta z} \tag{2.5}$$

where z is the space coordinate along the long axis of the cylinder, $P(z)$ is the probability of finding any monomer in a bin/disk centred around z, $n(z)$ is the total number of monomers found to be in the bin/disk around z throughout the simulation, n_{total} is the total number of monomers found in the entire cylinder throughout the simulation, and Δz is the width of the bin/disk. The bin extends from $z - \Delta z/2$ to $z + \Delta z/2$. Integrating $P(z)$ over all the bins gives 1.

Looking at such a plot, one can identify if there are any density fluctuations along the length of the cell. In normal circumstances, we expect a relatively flat density along the length of the cylinder that drops to 0 close to the edges. Figure 3.2d shows such a density curve plotted for each polymer separately over a single simulation snapshot. Departures from a flat curve are indicative of density variations that can be due to improper initialization or a consequence of the topology being used.

(ii) Single-Snapshot Monomer Density:

The above probability density is plotted by averaging over the entire initialization simulation. It is possible that certain anomalous density fluctuations get averaged out over the course of the entire run. Since we only take the last snapshot of the simulation as our mixed state, we can ignore the rest of the run when we want to study just the mixed state. In this way, we calculate the monomer density only based on the data within the last snapshot.

(iii) Sectional Monomer Density:

To study the density of the monomers along the radial directions, we divide the cylinder into different "sections" as shown in Figure 2.4. This quantity is the same as the monomer density along the long axis but is plotted separately for each "section". Comparing monomer densities for different sections can tell us about the differences along the radial direction. Figure 3.2a shows a typical plot of monomer densities in various sections.

Any higher density fluctuations along the z-axis or differences among the different sections can give an indication of anomalies that may have occurred during the shrinking procedure.

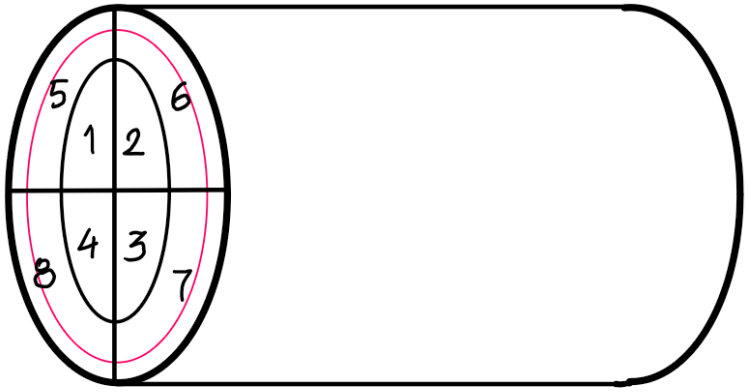

Figure 2.4: The cylinder is divided into 8 sections to calculate monomer density separately in each. The sections are made by dividing the cross-section of the cylinder into 4 sectors, and each sector is further divided radially into an inner and outer section. This division in the cross-section is extended longitudinally along the length of the cylinder. The numbers indicate the IDs of different sections. The pink circle indicates the threshold beyond which monomers feel the repulsion from the cylinder walls.

If the cylinder shrinks too fast, the monomers of the polymers would not have enough time to relax, which would lead to a much higher density close to the walls of the cylinder.

(iv) Radial Monomer Density:

To study the density variations more directly, we plotted the monomer density along the radial direction, as shown in Figure 3.2b. The radial probability density was calculated a little differently:

$$P(r) = \frac{n(r)}{n_{total}\, 2\pi r\, \Delta r} \tag{2.6}$$

The extra $2\pi r$ term is included to account for the increasing volume of bins at higher radii.

2.4.2 Time Series

The above monomer densities were plotted as an average over the entire length of the simulation. To capture any transient anomalies that might be missed in this averaging, we also calculate the time series of the centres of mass (CoM) of the polymers. More precisely, we plot the distance (along the long axis) between the centres of mass (CoMs) of the polymers as a function of the simulation time. We call this distance "CoM Distance" Figure 3.5c

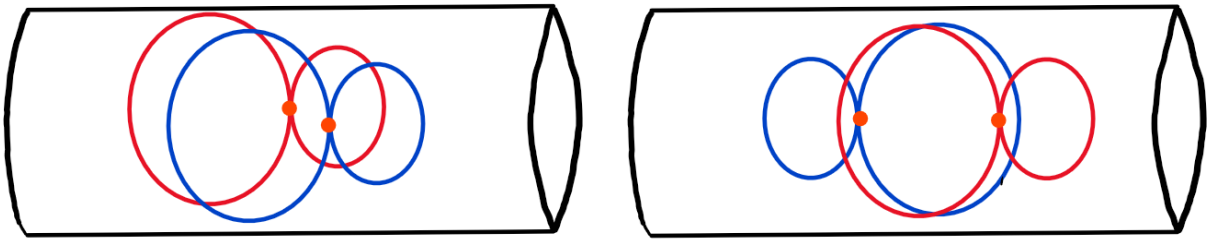

(a) (b)

Figure 2.5: The two different orientations that the polymers majorly occur in the cylinder in a mixed state. (a) shows a 'parallel' orientation where each polymer's small loop is on the same side, and their big loops are on the other side. (b) shows an 'antiparallel' orientation where each polymer's small loops are on opposite sides as are the big loops.

shows an example of such a trajectory.

In the case where we use an architecture more complicated than the ring Arc0, we also plot the z-coordinate of the CoM of different regions of each polymer as a function of time. For example, for Arc-1-10, the CoM of the big loop and the CoM of the small loops are plotted for each polymer (see Figure 3.2e). In addition to showing information about each individual region, it also tells us about the relative orientation of the two polymers in the mixed state. In all architectures with anisotropy, we have found that the polymers prefer to be either in 'parallel' orientation or 'antiparallel' orientation. The polymers are said to be parallel if their corresponding regions are close to each other along the long axis of the cylinder (see Figure 2.5a). In an antiparallel orientation, the corresponding regions are on opposite sides of the cylinder (see Figure 2.5b). If we were to draw a vector representing the anisotropy direction of a polymer, then the two polymer vectors are parallel in parallel orientation and antiparallel in antiparallel orientation. This orientation information will be useful while analysing the results.

In addition, these trajectories can give us information on the extent to which the polymers are mixed and any fluctuations in their degree of mixing represented by the CoM distance. In normal cases, for a mixed state, we expect the CoM Distance to be at most a fifth of the total cylinder length. In some simulations, the CoM Distance is much smaller than this limit.

2.4.3 Pair Correlation

We also calculated the pair correlation function $g(r)$, which gives information about the local structure of the system. It is given by the ratio of average monomer density at a radius r from a monomer to the average monomer density of the system [35]. Mathematically,

$$g(r) \;=\; \frac{\langle \rho(\mathbf{r}) \rangle_{|\mathbf{r}-\mathbf{r}'|=r}}{\rho} \tag{2.7}$$

where $\mathbf{r}'$ is the position of a chosen monomer, $\rho(\mathbf{r})$ is the density of monomers at the position $\mathbf{r}$, and ρ is the average monomer density in the system. The average $\langle\rangle_{|\mathbf{r}-\mathbf{r}'|=r}$ is taken over all monomers at various $\mathbf{r}'$s and over all $\mathbf{r}$ such that the distance between the monomer and $\mathbf{r}$ is r. Figure 3.3a gives an example of $g(r)$. A value of $g(r) = 1$ represents no special correlations between the chosen monomer and the monomers at a distance r. Such a value is attained in all fluid systems as long distances ($r >> 1$). A deviation from $g(r) = 1$ shows correlations between monomers at a separation of r due to inter-monomer forces [35]. The $g(r)$ shows peaks at a distance from a monomer where other neighbouring monomers are likely to occur. We also investigated $g(r)$ curves by ignoring the bonded neighbours from the average, which are shown in the orange and green curves in the figures. The orange curve shows the density of monomers belonging to the same polymer as the central monomer. Meanwhile, the green curve indicates the density of monomers belonging to the other polymer. This green curve is calculated by only considering distances between monomers of two different polymers.

If there were any unusual clusterings of the monomers due to the shrinking procedure of initialization, we should obtain anomalous peaks beyond the first one. The absence of such peaks indicates that the system is well "relaxed".

2.4.4 Checking for concatenations

Finally, we check whether there are any concatenations (like links in a metal chain) present between the two polymers or between subloops of the same polymer. We use a simple procedure to check for concatenations. We take the mixed state as a starting configuration and let the system simulate in free space (or in a very big box). Unconcatenated polymers would drift apart due to diffusion, whereas concatenated polymers would be forced to stay together due to their topological constraint. During the simulation, we observe whether

the polymers move apart, and thus, we can conclude whether they are concatenated or not. In all the simulations I have given, the two polymers always move apart, signifying no concatenations.

We perform this same procedure for the subloops of the complicated architectures we make. The only difference is that we delete the backbone of the polymer and track whether the now disconnected subloops move apart. Again, all the simulations showed that none of the subloops were concatenated with one another.

2.5 Finding Segregation Time

Starting from the mixed state obtained via one of the various procedures outlined in Section 2.3, we run a simulation where the polymers are allowed to evolve naturally. We disable the initialization constraints acting on the system at time $t = T_0$. As soon as the constraints stop acting, the polymers tend to evolve to a segregated state. We record the time after T_0 at which the polymers become segregated as the "segregation time".

But when exactly does a system of polymers transition from a mixed state to a segregated state? We impose a definite set of conditions that must be satisfied by the system of two polymers in order for them to be considered segregated. These conditions are quantitative, and thus, when two polymers segregate, they give us a precise time at which the segregation occurred.

We monitor the distance D_{COM} along the cylinder long axis between the centres of mass (COMs) of the two polymers to infer the segregation time. Loosely speaking, the polymers are considered mixed when D_{COM} is low and segregated when D_{COM} is high. When the mixing constraints are released, the D_{COM} naturally tends to grow till it reaches a maximum (see Figure 2.6). We use two successive conditions to check for segregation:

(i) We define a *first-crossing threshold* f that the D_{COM} must surpass at least once during the segregation simulation. The time T_f at which D_{COM} increases above f is recorded.

(ii) Once the above condition is satisfied, we calculate the time average of D_{COM} over a time window. The value of this average $\bar{D}_{COM}$ (denoted by a "bar" on top) must be above a threshold s that we define. The time average is taken starting from the time T_f over a time

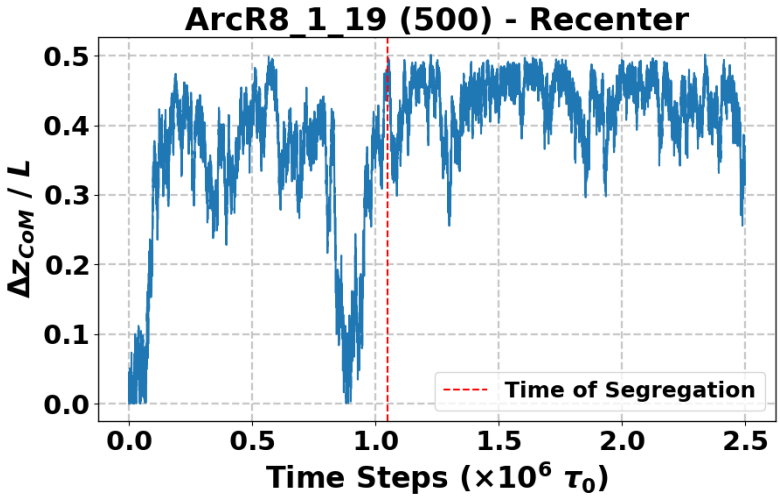

Figure 2.6: An example of the time series of the distance (along the z-axis) between the centres of mass of the polymers during segregation. The red dotted line indicates the time taken as the segregation time based on the segregation criterion.

window that spans half the duration of the entire segregation run or till the end of the run, whichever is shorter (see Figure 2.6). The value of s is slightly lower than f. This condition is imposed to ensure that the polymers stay separated after T_f.

The purpose of the second condition is to discard the cases in which the D_{COM} crosses the threshold due to a transient fluctuation and returns back below the threshold. Such a situation occurs in the case shown in Figure 2.6. If the D_{COM} falls much below the threshold within the window, then the event is not considered a segregation event.

At any step, if any of the conditions are violated, the whole process is performed again for the remainder of the simulation trajectory. In some cases, the two conditions remain unsatisfied even till the end of the simulation. The polymers are considered unsegregated in these runs and no segregation time is reported.

If the above conditions are satisfied for a simulation, then T_f is declared as the time of segregation for that run. Note that it is not necessary for T_f to be the first time when D_{COM} crosses f. T_f might be a subsequent time if condition (ii) is violated for the first event when D_{COM} surpasses f.

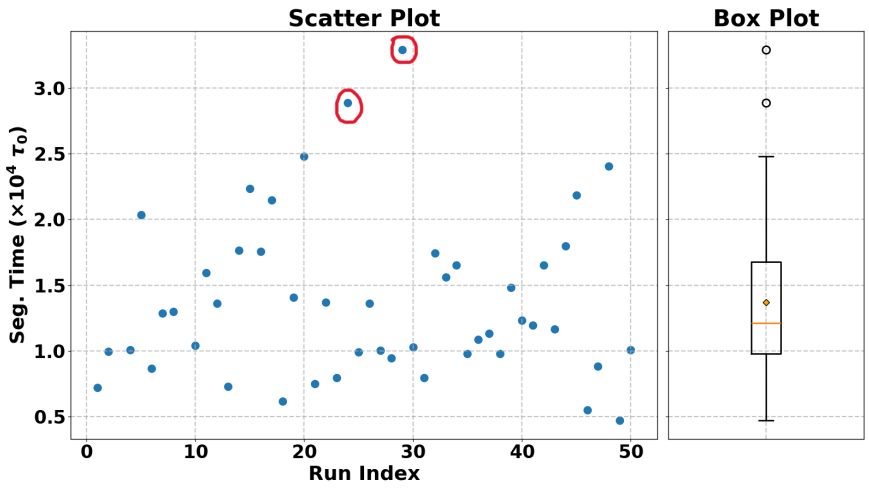

Figure 2.7: An example of the spread of segregation times obtained for a set of 50 independent simulations. On the left, a scatter plot of the data is plotted. On the right, the corresponding box plot is shown. Most of the data points lie within the 'box' and 'whiskers' of the plot, but certain outliers (circles in red in the scatter plot) are plotted as separate dots. The box plot also shows the median (orange line) and the mean (orange diamond).

2.6 Plotting Segregation Times

As described in the previous section, segregation times are measured from simulations. Fifty such independent simulations are run for each architecture to obtain a sample of 50 segregation times for the same architecture. The mean or median and the spread of this set of times can be compared across architectures to test for differences. We visualise the data in terms of Tukey's box-and-whisker plots (or simply box plots) [34]. As explained below, representing the data in this format makes comparisons easier.

The box plot summarizes the dataset in terms of the three quartiles: the 25th percentile, the median, and the 75th percentile. Figure 2.7 shows an example of a dataset and its box plot. A box plot comprises a box representing the central portion of the data, "whiskers" above and below the box, and "outliers". The upper and lower edges of the box are the 25th percentile and the 75th percentile, respectively. The median is represented as a line cutting through the box between the lower and upper edges. The height of the box is the difference between the upper and lower quartiles, also known as the "Inter Quartile Range (IQR)". The two whiskers extend from either edge of the box in the up and down directions till some upper and lower threshold. These thresholds are taken as 1.5 $\times$ IQR above and below the

upper and lower edges of the box, respectively. Finally, any points not lying between these two thresholds are termed outliers and are represented as individual points or circles.

The height of the box and the height between the whiskers indicate the spread of the data. If any outliers are present, they indicate data points with extreme values that are quite far away from the rest of the data. I chose such a representation for the segregation times because of the presence of such outliers in my dataset (as shown in red circles in Figure 2.7). With such outliers and skewed data sets, a comparison based on just the mean and standard deviation is often inconclusive. The box plot clearly separates the outliers from the rest of the data and also gives a visual indication of the skewness. For all the architectures I have considered, I have plotted the segregation times as box plots next to each other to make comparison easier.

2.7 Statistical Test

To quantify the difference between the segregation times of different architectures, we employ a simple statistical test. We compare the mean segregation time of two architectures using the "*two-tailed t-test*". We briefly explain the essence of this statistical test below. The full explanation can be found by consulting Chapters 19 and 20 of [34].

We compute the difference between the means μ_1 and μ_2 of the two sets of the data corresponding to different architectures. The hypothesis we want to test for is $\mu_1 - \mu_2 = 0$. If the two means are similar, then the two sets of data cannot be said to be statistically different. However, if the value of the difference of means is very far away from zero, then we can say that the two data sets are statistically distinct. How far away does the value need to be for the hypothesis to be considered untrue? This distance is determined by the natural variation (standard deviation) of the means. In short, if the difference value is located at distance of atleast two or three times the natural variation from zero, the difference is considered significant.

The procedure of testing this hypothesis quantitatively is executed while performing the '*t-test*'. In particular, the *t-test* is used to compare datasets whose natural variations are unknown, which is the case for our data. W use a slightly modified version, the '*two-tailed t-test*', which checks whether the difference of means is far away on both sides of zero.

It directly computes the *p-value*, which signifies the probability that the two datasets are statistically identical. Thus, if the *p-value* is low, we can claim that the two data sets are different. In this thesis, we use the significance threshold $\alpha = 0.05$ below which our *p-value* must be to consider the means distinct. In Section 3.9, we give the computed *p-values* for some of our data. Google Sheets was used to perform these *t-tests*.

There is a caveat while using these statistical tests. Such tests are based on mathematical models which rely on certain assumptions being true. For example, the *t-test* assumes that the means of the datasets is Gaussian distributed. This assumption is valid as long as there are a substantial number (> 30) of datapoints in the data set. However, there should not be any extreme outliers present. This last assumption may not be strictly true for some of the segregation times we measured. Thus, in those cases, the test results may not be reliable, and should be taken with a pinch of salt.

Chapter 3

Results

In this chapter, we state the observations and results we obtained from running the simulations of two polymers in confinement. As described in Section 2.3, we use several initialization procedures to create a mixed state of two polymers. For each of these different procedures, we study segregation independently. This chapter is divided into sections, with each section corresponding to a particular initialization procedure used. The first four sections discuss the case of polymers with 200 monomers, followed by four sections that discuss the case of polymers with 500 monomers each. In each section, we provide details about the validity of the mixed states and the trends in the resulting segregation times.

3.1 *Recenter*

To remind the reader, the *Recenter* procedure constrains the centres of mass of the two polymers to be confined to the equatorial plane ($z = 0$ plane) of the cylinder.

3.1.1 Validity of Mixed States

Figures 3.1 and 3.2 show the different quantities calculated and plotted to give information about the mixing procedure and the final mixed state. Figure 3.1 corresponds to the case of Arc0 (ring) polymers, while Figure 3.2 is for Arc-1-10 polymers. These quantities were

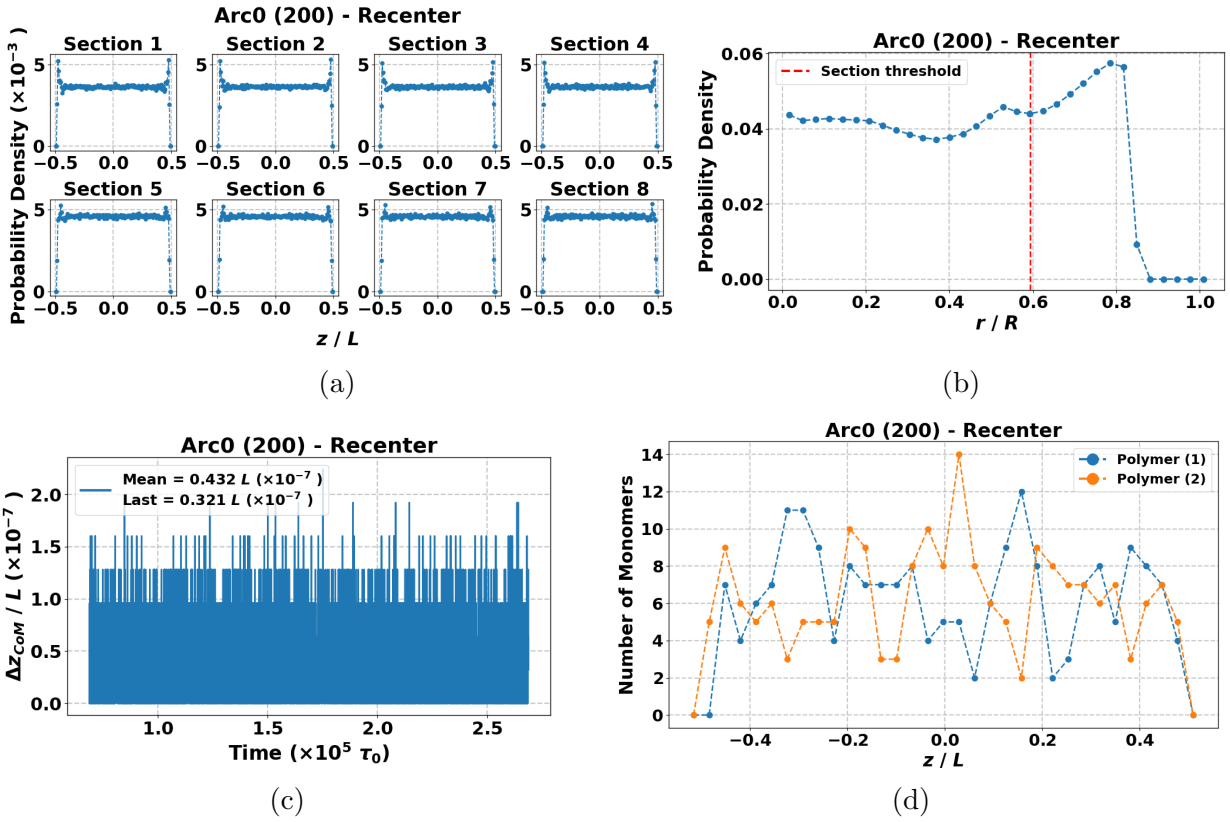

Figure 3.1: Various plots showing the state quantities for the mixed Arc0 (200) ring polymers during the *Recenter* procedure. (a) Monomer density in different sections, (b) Monomer density along the radial direction, (c) Time series of the distance between Polymer centres of mass (CoMs), and (d) Monomer density from the mixed state snapshot. Plots (a) and (b) show that monomers are roughly uniformly distributed throughout the cylinder. Plots (c) and (d) show that the two polymers are well-overlapped along the long axis of the cylinder.

described in Section 2.4.

Firstly, we check for any artefacts caused by the shrinking of the cylinder. Subfigures (a) and (b) in both figures show the monomer density in different sections along the long axis and along the radial direction, respectively (see Section 2.4.1 for how these quantities are calculated). The density is roughly constant along the cylinder axis (z-axis) for all sections, signifying all monomers are uniformly distributed. There is a slight difference in the value of the densities in the inner and outer sections. This difference is due to a clustering of monomers close to the wall, which leads to a slightly higher density in the outer sections. This wall effect is more evident in the radial density plot, where a peak exists close to the wall beyond which the density drops. A second smaller peak also exists away from the wall,

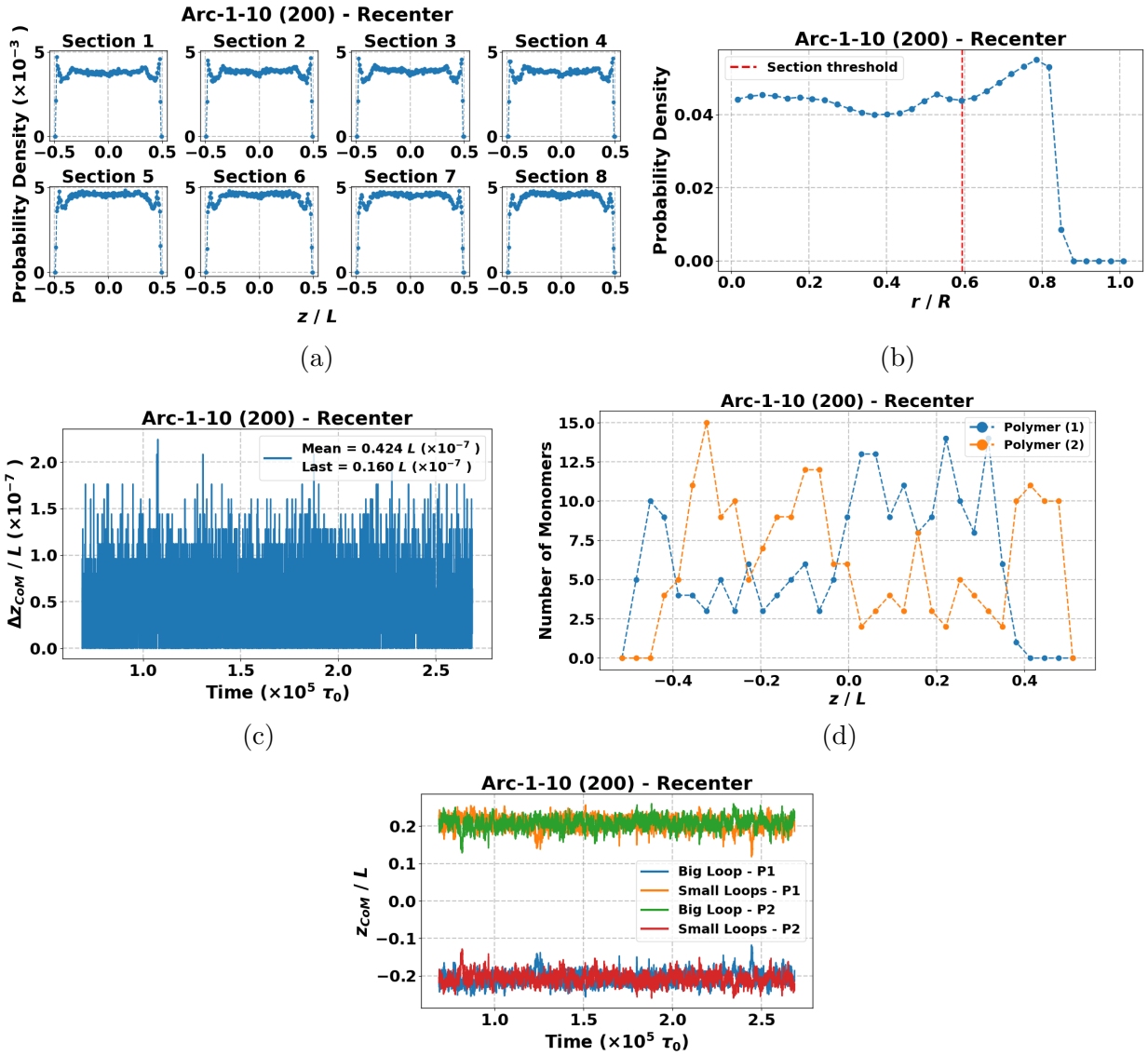

Figure 3.2: Various plots showing the monomer distribution for the mixed Arc-1-10 (200) polymers during the *Recenter* procedure. (a) Monomer density in different sections, (b) Monomer density along the radial direction, (c) Time series of the distance between Polymer centres of mass (CoMs), (d) Monomer density from the mixed state snapshot, and (e) Time series of the CoM of each region of the two polymers. Plots in (a) and (b) show that monomers are roughly uniformly distributed throughout the cylinder. Plots (c) and (d) show that the two polymers are well-overlapped along the long axis of the cylinder. Plot (e) highlights that the two polymers are in antiparallel orientation. The ring polymer has no sub-polymer regions like in Arc-1-10. Thus, a plot corresponding to (e) was not plotted in Figure 3.1 for ring polymers.

which signifies the increase in density due to the clustering of a second layer of monomers on top of the first layer. The radial density plot is divided into the inner and outer sections by a red dotted line.

Figures 3.1c and 3.2c show the distance z_{CoM} between the centres of mass (CoMs) of the two polymers along the cylinder axis as a function of time. Due to the constraint imposed, the distance is supposed to be exactly 0, which is the ideal condition for mixed polymers. Indeed, the subfigures show very small distances ($\sim 10^{-6}$), which are due to floating point errors exacerbated by numerical calculations. In Figure 3.2e, we show the CoM trajectory of different 'regions' of the two Arc-1-10 polymers. We define regions (not to be confused with sections) as subsets of monomers in a single polymer. In the case of *multiple-looped* architectures, each polymer is divided into two regions: the monomers constituting the small loops and the monomers constituting the single big loop. The centre of mass of each region is calculated separately and plotted in Figure 3.2e. It is seen that the big loop of a polymer is mixed with the small loops of the other polymer in what we call an 'antiparallel' orientation. A similar figure is not plotted for the Arc0 polymer since all monomers are identical in a ring. It does not make sense to divide the ring into different regions.

Figures 3.1d and 3.2d show the monomer density of the two polymers in the mixed state, calculated over the last frame of the mixing simulation. For Arc0, the distribution for both polymers extends to the full length of the cylinder, but the density drops close to the walls as expected. The peaks and valleys are transient density fluctuations along the cylinder length. Despite these fluctuations, the plot shows that both polymers are exploring the entire length of the cylinder. For Arc-1-10, the densities are not uniform over the length of the cylinder. One side of the cylinder has a higher density of one polymer, with a lower density of the other polymer. The other side of the cylinder is mirrored with the cases flipped. This is due to the antiparallel orientation of the polymers; the higher-density region corresponds to the small loops of either polymer, and the low-density region corresponds to the big loops. Despite this disuniformity, it can be seen that both polymers show significant overlap, which suffices to call the state mixed.

Figure 3.3 shows the pair correlation functions for Arc-1-10 polymers in the mixed and segregated states. For both cases, The total pair correlation function shows a strong peak close to 1 σ and another small peak close to 2 σ. The first tallest peak is indicative of the bonded neighbours of a particular monomer, which is present for each and every monomer.

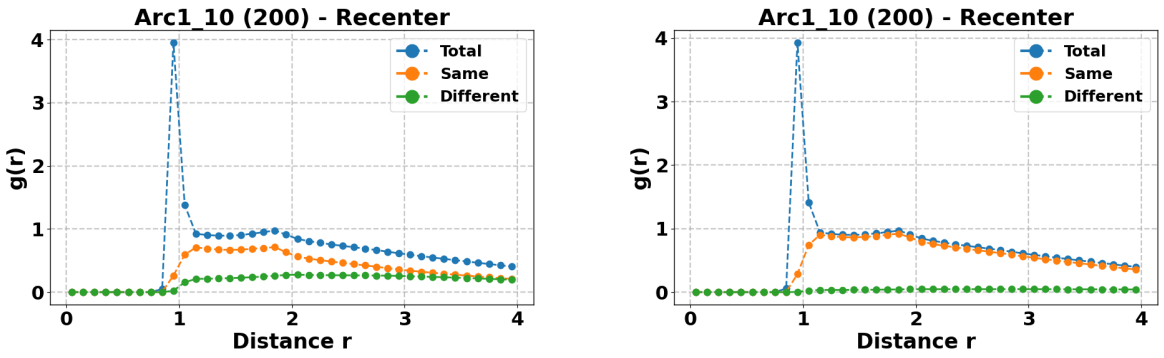

(a) (b)

Figure 3.3: Pair Correlation Functions $g(r)$ plotted for the (a) mixed state and (b) segregated state of two Arc-1-10 (200) polymers. The blue curve gives the actual $g(r)$. The orange curve gives the $g(r)$ on only considering monomers from the same polymer as the central monomer. The green curve gives the $g(r)$ on only considering the monomers from the other polymer.

Hence, this first peak is very strong. The second peak indicates the next set of neighbours, which are not permanent. Ideally, in an infinite volume of fluid, the pair correlation function must approach 1 at long distances in an equilibrated system. However, in the examples in Figure 3.3, the $g(r)$ decays slowly at longer distances. This is due to the finite size of the cylinder in which the $g(r)$ is being calculated.

The curve labelled 'Different' shows the distribution of neighbours from the other polymer. For the mixed state, the 'Different' curve is zero at short distances but finite at longer distances. This means that monomers from the other polymer are present around any monomer of a given polymer on average; this is a sign of the state being mixed. In contrast, for the segregated case, the 'Different' curve is almost 0 at all distances within the cylinder diameter. This implies that very few monomers are close to monomers of the other polymer, as is expected.

We performed all of the above analyses for all runs of all the considered topologies. The plots for other architectures are similar, with Arc0 and Arc-1-10 representing the two extreme cases of the bunch. As can be seen from the monomer density plots, Arc0 seems to be better mixed than Arc-1-10. The reason for this will become evident when we discuss the trends of segregation times. For brevity, in the subsequent sections, only the plots for Arc-1-10 (the most extreme case) are shown. Further, the pair correlation functions are similar across all procedures; thus, they are omitted in the following sections.

Lastly, we check whether the two polymers or their internal subloops are concatenated with one another. This is checked via the procedure highlighted in Section 2.4.4. We found no concatenations for all runs of all architectures and across all initialization procedures.

3.1.2 Segregation Times

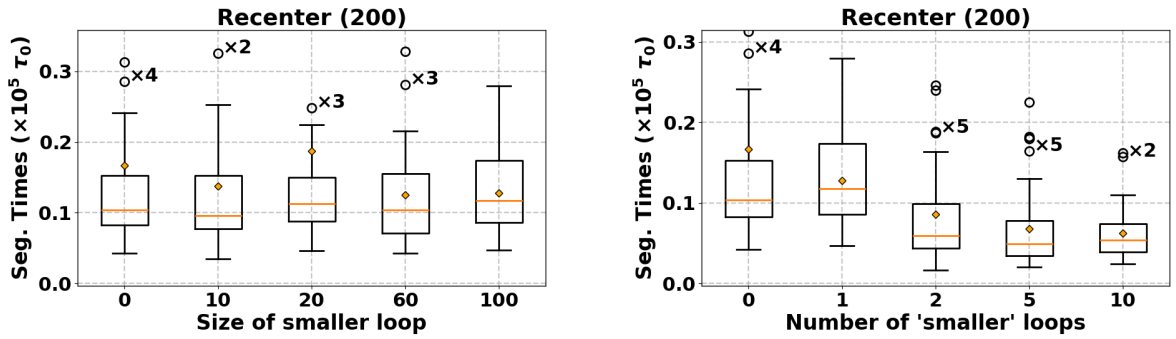

(a) (b)

Figure 3.4: The segregation box plots comparing various architectures for the *Recenter* procedure. Each box plot has an orange diamond that indicates the mean segregation time for that architecture. The numbers written close to the outliers (if any) indicate the total number of outliers for that architecture. Some outliers are not explicitly shown for clarity of the rest of the data. (a) shows the segregation times' comparison for *single-looped* topologies with varying sizes of the smaller loop (total monomers in the polymer remain constant). (b) shows the comparison for *multiple-looped* topologies with varying number of smaller loops.

In Figure 3.4a, we present the segregation times of various pairs of architectures, each having a single small subloop in addition to the big subloop. The plot compares the spread of the segregation times obtained over 50 independent runs via boxplots. As can be seen in the figure, there is not much difference in the means or medians or spreads of different architectures as the subloop size is changed. Thus, changing the size of the subloop in a *single-looped* polymer does not significantly affect the segregation times of the pair of polymers.

On the other hand, Figure 3.4b shows the segregation times for architectures with a different number of subloops. As shown in the *single-looped* case, there is not much difference in the distributions for Arc0 and Arc-1-1 (also known as ArcR8-1-1). In contrast to the *single-looped* case, the medians and the spread of the segregation time distributions decrease

with an increase in the number of subloops present. The effect is seen clearly when moving from Arc-1-1 (1 subloop) to Arc-1-2 (2 subloops). Beyond Arc-1-2, the segregation time distribution does not decrease much further in terms of median and spread. This implies that the segregation process speeds up with an increase in the number of loops.

This speed-up is a consequence of the same mechanism that drives segregation: entropy maximization. As we discussed, the polymers can access a lower number of conformations when they are overlapped in confinement and, thus, tend to repel. Similarly, even subloops feel the same repulsion when overlapping with other subloops. The more subloops there are in both polymers, the stronger the tendency to segregate. Hence, we see a decrease in segregation time as the number of loops increases.

3.2 *Fixing-Bonding*

As per this procedure, the initial mixed states were created by fixing two monomers in the equatorial plane of the cylinder and introducing two interpolymer bonds at two opposite poles of the polymer.

3.2.1 Validity of the mixed states

Figure 3.5 shows the various quantities plotted for the mixing simulation for two Arc-1-10 polymers. Figure 3.5a shows the monomer density in the inner and outer sections of the cylinder. The left and the right halves of all plots show a stark difference. The left side is relatively flat in all sections, similar to the case for *Recenter*. However, the right side shows alternating peaks and valleys starting from the equator and dying out towards the walls. The reason for such a feature is the initialization condition of fixing the two monomers in space. This causes the surrounding bonded monomers to occupy the space close to the equator. The monomers that are fixed divide the polymer into two parts: one with the single big loop and the other with multiple small loops. Due to the constraints imposed, it is difficult for monomers from one part to diffuse to the other. The small loops of both polymers are forced to occupy the space on the right of the equator due to this constraint. As a result, the polymers are forced to be in a 'parallel orientation' with small loops on one side and the

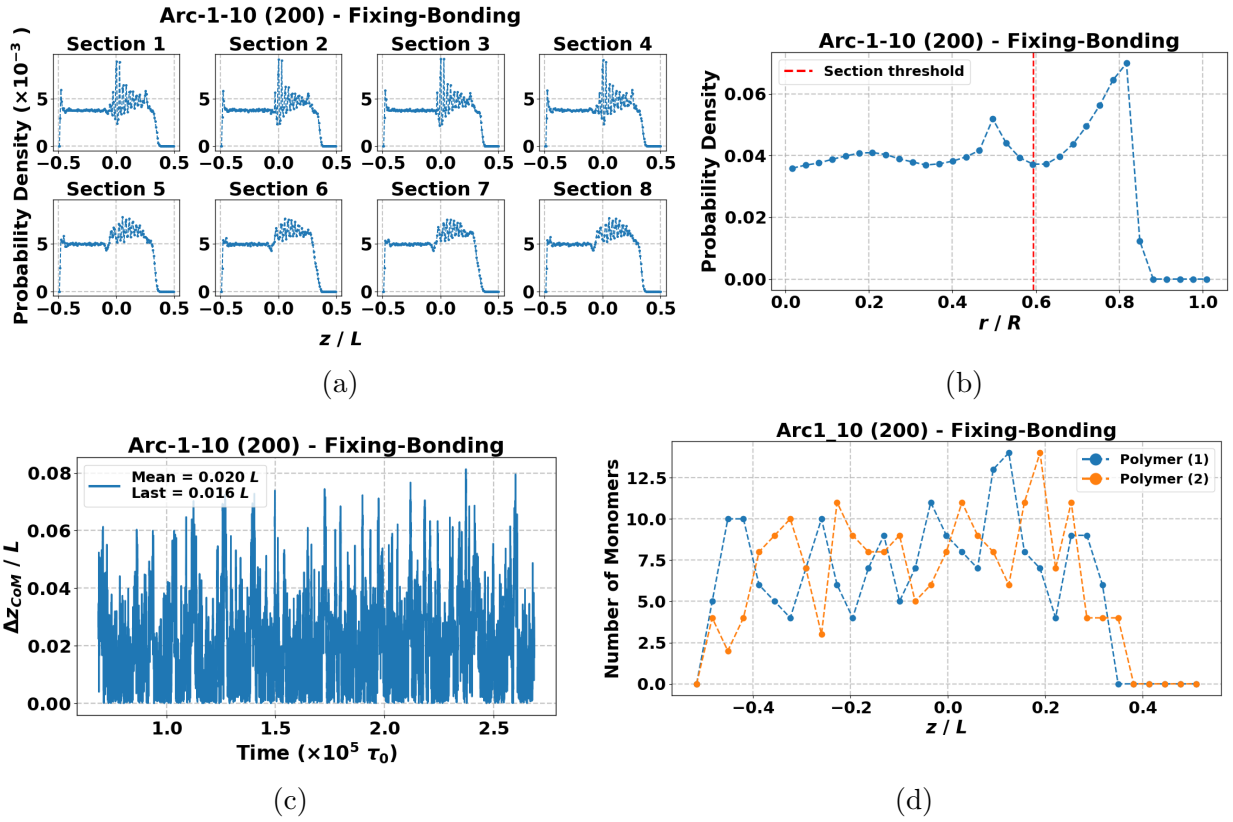

Figure 3.5: Various plots showing the monomer distribution for the mixed Arc-1-10 (200) polymers during the *Fixing-Bonding* procedure. (a) Monomer density in different sections (b) Monomer density along the radial direction (c) Time series of the distance between Polymer centres of mass (CoMs) (d) Monomer density from the mixed state snapshot. Plots (a) and (b) show how the monomers are distributed throughout the cylinder. Plots (c) and (d) show that the two polymers are well-overlapped along the long axis of the cylinder.

big loops on the other. The high number of cross-links causes a cluster of monomers on the right, which cannot spread out or move far away from the equator. Hence, the monomers occupy a small volume close to the equator, leading to a high-density region.

The peaks and valleys are features of this high density, which indicates the compact packing of the monomers in successive layers around the fixed monomers at the equator. On the left side of the equator, the big loops of the Arc-1-10 architecture lie. They are more spread out over the left half of the cylinder, as reflected in the flat curve. Note that there is a slight difference in the peak height between the inner and outer sections. The inner sections host the fixed monomers, which contribute to the high monomer density at the centre of the cylinder. The outer regions are devoid of these fixed monomers at all times and hence show

a lower density at the centre.

Figure 3.5b shows the radial density with features reminiscent of the *Recenter* case. A peak close to the wall exists due to the wall effect. However, the second peak away from the wall is sharper than in *Recenter*. The constraint fixes a set of four monomers at $R/2$ from the centre; thus, we see the peak at $r/R = 0.5$. Here, R is the radius of the cylinder, and r is the radial coordinate where we calculate the monomer density. The peak due to the second layer of monomers from the wall has merged with the stronger peak due to the fixed monomers. Also note that since the monomers are fixed at $R/2$, some of the connected monomers are pulled away from the region close to the central axis, leaving a slight dip at $r = 0$.

Figure 3.5c shows the time evolution of the distance along the cylinder axis between the centres of mass (CoMs) of the two polymers. This distance never goes beyond $0.1L$ (where L is the cylinder length). Thus, the CoMs are quite close together along the cylinder axis.

Figure 3.5d shows the monomer density from a single snapshot. Both polymers overlap to a good extent; however, they fall off before reaching the wall on the right side. As explained earlier, this is due to the constraints keeping the small-looped regions close to the equator. Despite the anomalous density fluctuations introduced by the constraints, the polymers are well-overlapped and can be considered mixed.

3.2.2 Segregation Times

Figures 3.6a and 3.6b show the comparisons of the segregation time spreads for *single-looped* and *multiple-looped* architectures respectively initialized using the *Fixing-Bonding* procedure. Both cases are quite similar to the *Recenter* case. The segregation times for *single-looped* architectures do not change significantly on changing the size of subloops. In contrast, the segregation times for *multiple-looped* architectures decrease with the increase in number of loops beyond 2.

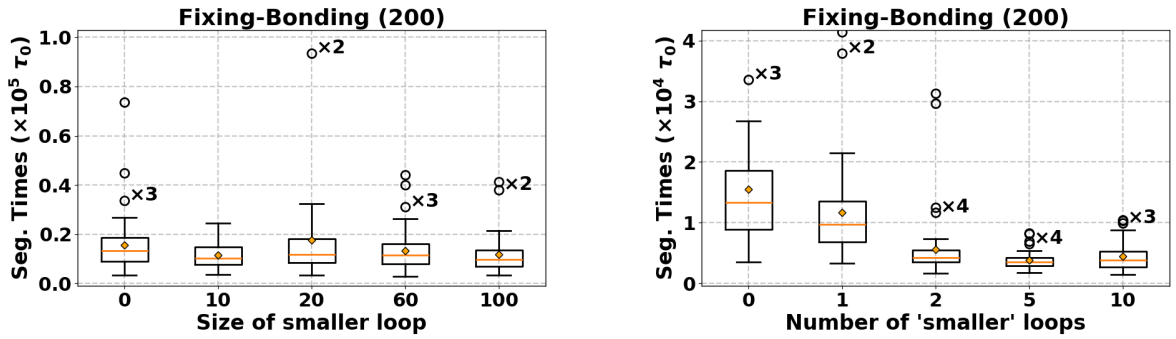

(a) (b)

Figure 3.6: The segregation box plots comparing various architectures for the *Fixing-Bonding* procedure. Each box plot has an orange diamond that indicates the mean segregation time for that architecture. The numbers written close to the outliers (if any) indicate the total number of outliers for that architecture. Some outliers are not explicitly shown for clarity of the rest of the data. (a) shows the segregation times' comparison for *single-looped* topologies with varying sizes of the smaller loop (total monomers in the polymer remain constant). (b) shows the comparison for *multiple-looped* topologies with varying number of smaller loops.

3.3 *Replication-like*

This section lists the simulation data and results obtained from the mixed states initialized via the *Replication-like* procedure. In this procedure, each and every monomer of a polymer was linked to the corresponding monomer of the other polymer via an interpolymer cross-link. Note that these constraints force the polymers to be in a parallel orientation.

3.3.1 Validity of mixed states

Figure 3.7a shows the monomer density in various sections of the cylinder. All of them show an asymmetric distribution with a higher density on one side and a slightly lower density on the other side. The high-density region comprises the small-looped regions of both polymers, while the big-looped region comprises the low density on the other side. There is a slight increase in the density throughout the cylinder, going from the inner sections to the outer sections. This is more clearly evident in the radial density (Figure 3.7b, which shows a bump close to the wall due to the wall effect. Away from the wall, there are small peaks corresponding to the clusterings of monomers at that radial distance. Interestingly, the

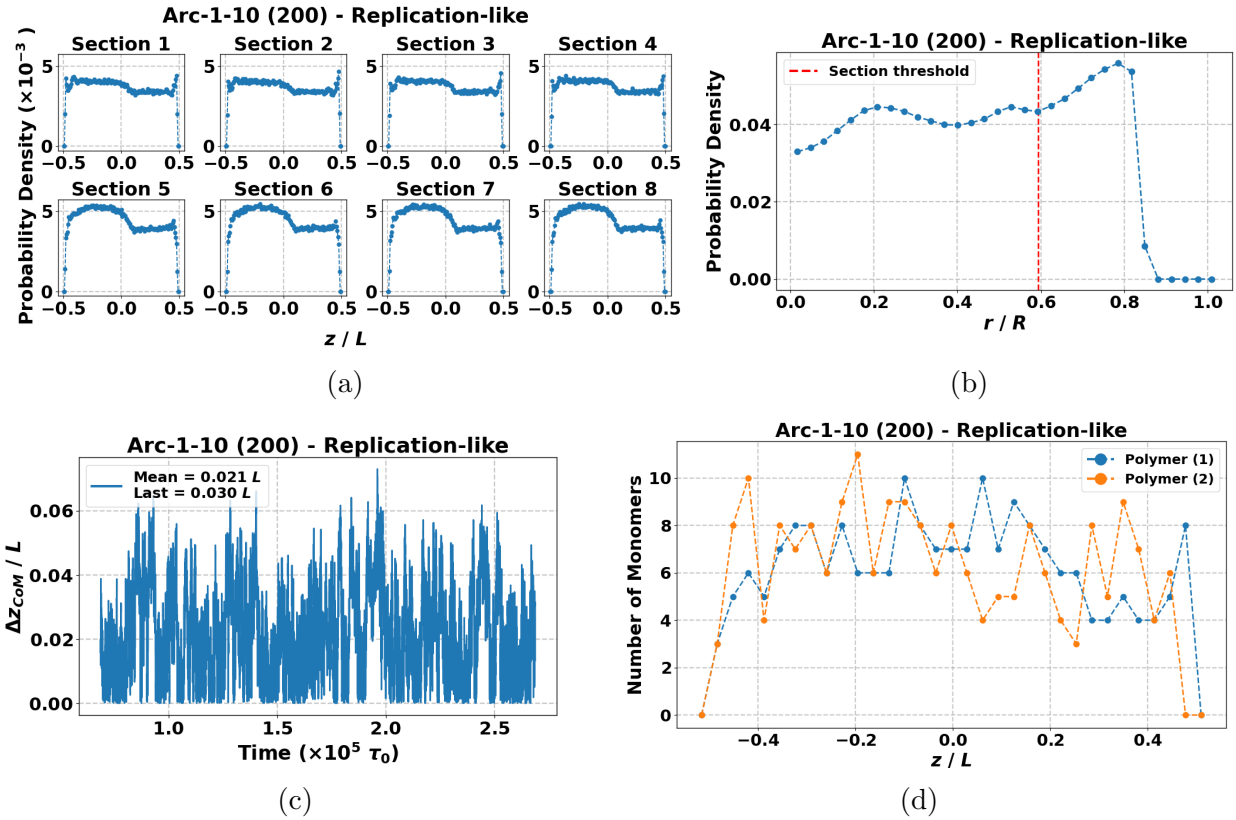

Figure 3.7: Various plots showing the state quantities for the mixed Arc-1-10 (200) polymers during the *Replication-like* procedure. (a) Monomer density in different sections (b) Monomer density along the radial direction (c) Time series of the distance between Polymer centres of mass (CoMs) (d) Monomer density from the mixed state snapshot. Plots (a) and (b) show how the monomers are distributed throughout the cylinder. Plots (c) and (d) show that the two polymers are well-overlapped along the long axis of the cylinder.

farthest peak from the wall corresponds to the monomers that are at a distance of 3σ (the equilibrium bond length of the interpolymer cross links). The high density of monomers at the walls causes a correspondingly high-density region 3σ away due to the constraints imposed.

Figure 3.7c shows the distance z_{CoM} between the centres of mass of the polymers along the cylinder axis. Throughout the mixing simulation, z_{CoM} does not rise beyond 0.1 times the total length of the cylinder. Thus, the centres of mass are quite close to each other along the cylinder axis.

The monomer density of a single snapshot is shown in Figure 3.7d. Along with the CoM

time series, this confirms that the polymers are overlapped to a good extent and justifies calling them mixed.

3.3.2 Segregation Times

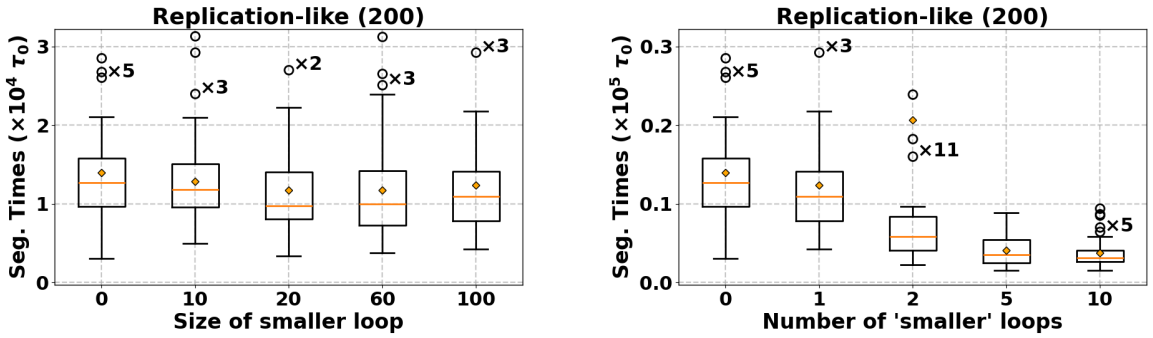

(a) (b)

Figure 3.8: The segregation box plots comparing various architectures for the *Replication-like* procedure. Each box plot has an orange diamond that indicates the mean segregation time for that architecture. The numbers written close to the outliers (if any) indicate the total number of outliers for that architecture. Some outliers are not explicitly shown for clarity of the rest of the data. (a) shows the segregation times' comparison for *single-looped* topologies with varying sizes of the smaller loop (total monomers in the polymer remain constant). (b) shows the comparison for *multiple-looped* topologies with varying number of smaller loops.

The segregation times' comparisons are shown in Figures 3.8a and 3.8b corresponding to *single-looped* and *multiple-looped* architectures, respectively. Again, as in the previous two cases, the *single-looped* architectures did not show a significant difference on changing the subloop sizes. The *multiple-looped* architectures showed the usual trend of decreasing segregation times with an increase in the number of loops beyond 2. However, the architecture with two loops showed a slightly higher spread than all of the other architectures, as indicated by the variation in outliers. Such a high variation in segregation time is attributed to entanglements or 'threadings', which will be explained in more detail in the next section for the *Mutual Attraction* procedure.

3.4 *Mutual Attraction*

The *Mutual Attraction* procedure introduces an attractive potential between monomers belonging to different polymers.

3.4.1 Validity of mixed states

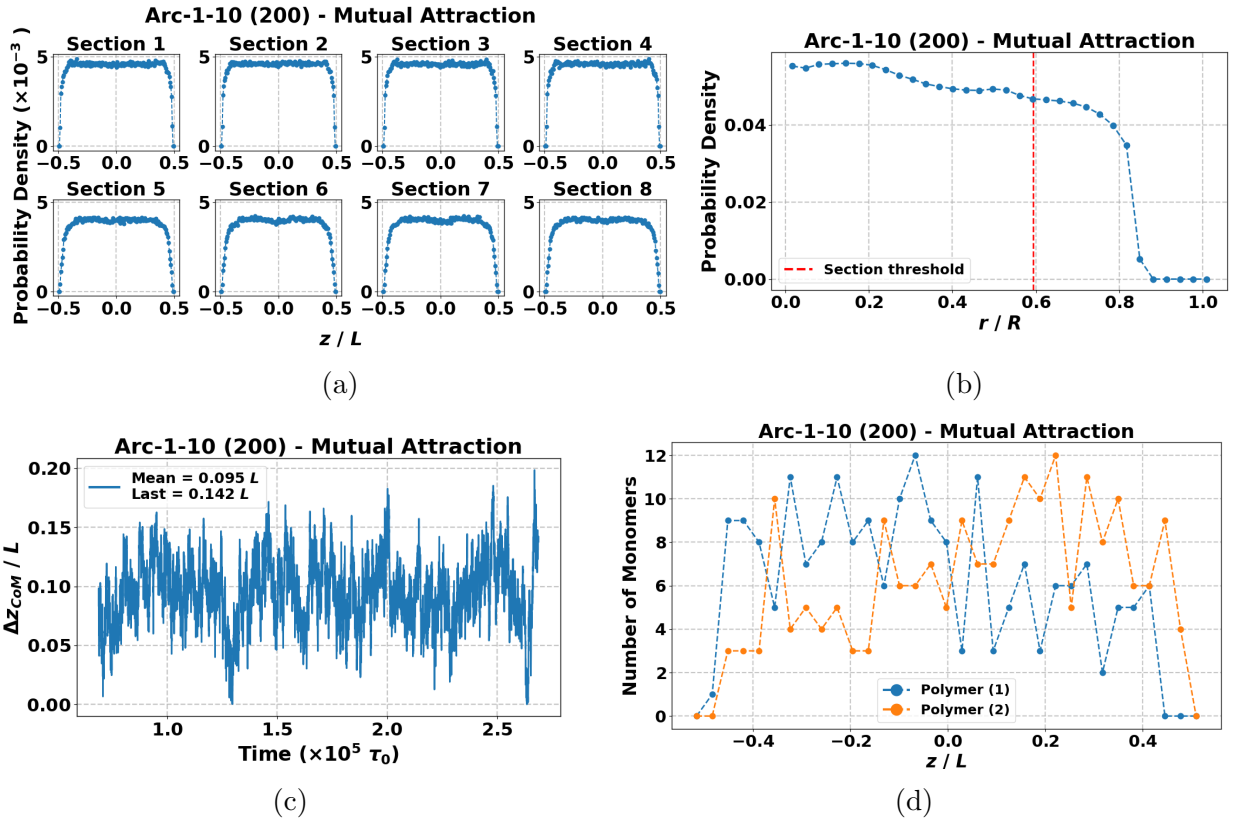

Figure 3.9: Various plots showing the state quantities for the mixed Arc-1-10 (200) polymers during the *Mutual Attraction* procedure. (a) Monomer density in different sections (b) Monomer density along the radial direction (c) Time series of the distance between Polymer centres of mass (CoMs) (d) Monomer density from the mixed state snapshot. Plots (a) and (b) show how the monomers are distributed throughout the cylinder. Plots (c) and (d) show that the two polymers are well-overlapped along the long axis of the cylinder.

In Figure 3.9a, we show the monomer density of the system in different sections. In all of the sections, the density is mostly uniform along the length of the cylinder. However, a difference from previous initialization procedures is that there is no increase in density close

to the walls. Instead, the monomer density falls off at the walls without showing a peak. In the previous simulations, a peak was present close to the walls, signifying the clustering of monomers. This was essentially due to the mutual repulsion between monomers, which pushed them against the walls. In the present case of *Mutual Attraction*, there is a mutual attraction across polymers. This attraction favours the clustering of the monomers among themselves rather than against the walls. Hence, no wall effect was seen in these simulations. As a consequence, the density in the inner sections (away from the walls) is higher than the density in the outer sections. The radial density plotted in Figure 3.9b confirms the absence of the wall effect in the radial direction. The density is maximum close to the central axis of the cylinder and gradually decreases when moving towards the walls.

Figure 3.9c shows the centre of mass distance z_{CoM} between the two polymers along the cylinder axis. Despite the attraction, this procedure seems to be the worst at keeping the centres of mass together. z_{CoM} seems to be centred around $0.1L$, but transiently cross $0.2L$ at times. However, it still remains less than half the value at segregation.

Despite the high value of z_{CoM}, it can be seen in Figure 3.9d that the polymers are well overlapped along the length of the cylinder. Hence, we can consider them to be sufficiently mixed.

3.4.2 Segregation Times

The comparisons of segregation times for *single-looped* and *multiple-looped* architectures are given in Figures 3.10a and 3.10b, respectively. Like the previously discussed procedures, the *single-looped* architectures did not show significant differences on changing the size of the subloops. In contrast with the other procedures, the trend for the *multiple-looped* architecture was quite different for *Mutual Attraction*. The key difference was the high spread in the segregation times for the Arc-1-2 architecture with two small subloops and a big subloop. As can be seen in Figure 3.10b, the spread and mean are higher than any of the other architectures.

On further investigation, we found that here, the segregation time is not just being affected by the entropic force due to the subloops. In addition, the entanglements or 'threadings' between the two polymers are slowing down segregation. We call two polymers en-

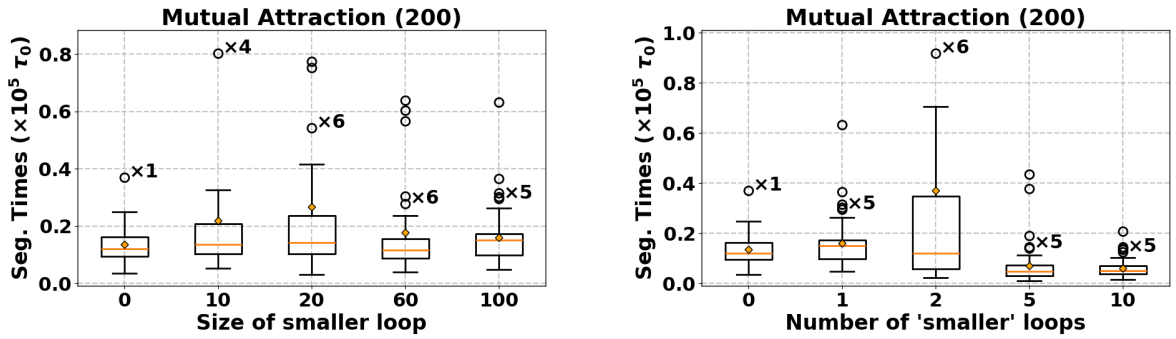

(a) (b)

Figure 3.10: The segregation box plots comparing various architectures for the *Mutual Attraction* procedure. Each box plot has an orange diamond that indicates the mean segregation time for that architecture. The numbers written close to the outliers (if any) indicate the total number of outliers for that architecture. Some outliers are not explicitly shown for clarity of the rest of the data. (a) shows the segregation times' comparison for *single-looped* topologies with varying sizes of the smaller loop (total monomers in the polymer remain constant). (b) shows the comparison for *multiple-looped* topologies with varying number of smaller loops.

tangled or 'threaded' when the contour of one polymer intersects the area enclosed by the contour of the other polymer.

Figure 3.11 shows two such polymers and highlights where the polymers are threaded. This is much like the case when a string is threaded through a needle's hole. Note that the polymers are still not concatenated, and such threadings can be removed just by the polymer motion without breaking any bonds.

The segregated state of polymers has unentangled polymers. To reach this state, any threadings must be removed or 'resolved'. Overcoming this obstacle may take some time. Thus, when the polymers are under confinement, such threadings can slow down the segregation of the polymers.

We found that polymers were threaded in a lot of the mixed states produced by the *Mutual Attraction* procedure, with an especially high number of runs for Arc-1-2. As a result, a lot of the runs of Arc-1-2 polymers showed a high segregation time, thus increasing the spread, as seen in the box plots.

The underlying reason for the introduction of such entanglements is the initialization

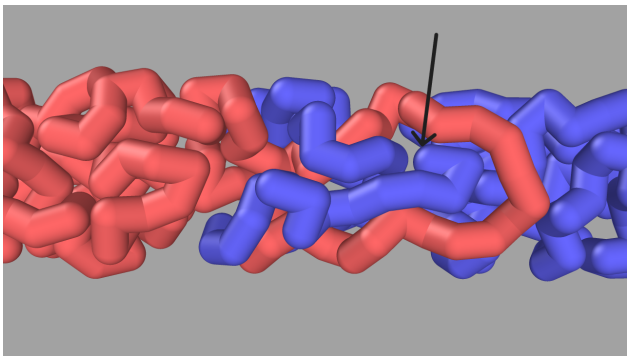

Figure 3.11: A section of a snapshot of two ArcR8-1-19 polymers clearly displaying threading. The red and the blue curves represent each polymer. It can be seen that the blue polymer has penetrated the area enclosed by the red polymer at the place indicated by the black arrow. The snapshots were visualised using OVITO [36].

procedure itself. The attraction introduced gives the monomers a good incentive to be surrounded by monomers from the other polymer. Such a favourable state can be achieved in entangled polymers. There was no such energetic incentive in other initialization procedures, so such entangled states were rarer.

Despite our hopes, this case makes it clear that the initialization procedure can affect the segregation time.

3.5 *Recenter*: 500 monomers

Here, we show the data obtained for a system with longer polymers of 500 monomers each. The mixed state was obtained using the *Recenter* procedure.

3.5.1 Validity of mixed states

Much like the case of 200 monomers, Figure 3.12 shows the various quantities plotted to ensure the validity of the mixed state for the Arc-1-10 polymers. Figure 3.12a shows the monomer distribution in different sections. It is similar to the 200-monomer case in the sense that the inner regions have a slightly lower density than the outer regions. This is confirmed in the radial monomer density plotted in Figure 3.12b. Like in the 200-monomer case this is

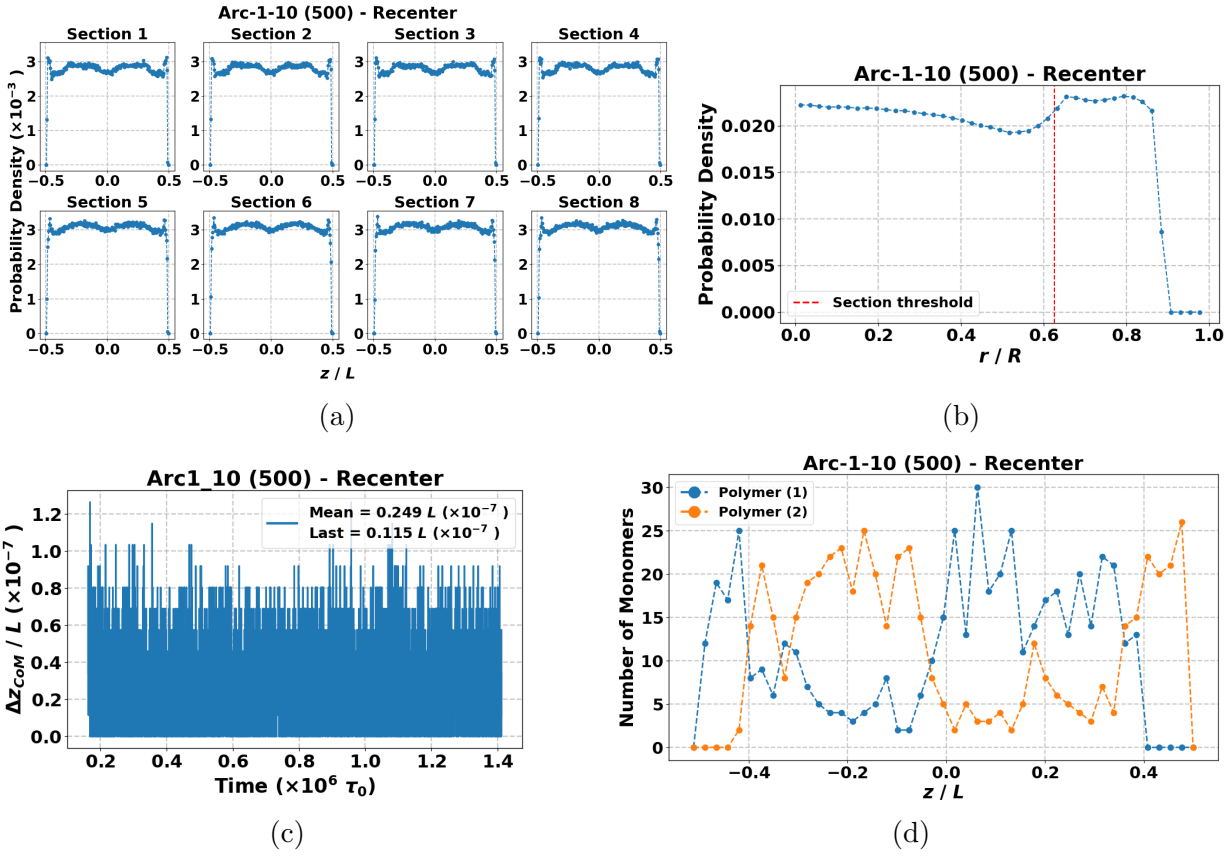

Figure 3.12: Various plots showing the monomer distribution for the mixed Arc-1-10 (500) polymers during the *Recenter* procedure. (a) Monomer density in different sections (b) Monomer density along the radial direction (c) Time series of the distance between Polymer centres of mass (CoMs) (d) Monomer density from the mixed state snapshot. Plots (a) and (b) show how the monomers are distributed throughout the cylinder. Plots (c) and (d) show that the two polymers are well-overlapped along the long axis of the cylinder.

a consequence of the wall effect, however the peak is spread out over a longer radial distance.

The rest of the plots, namely the centre of mass (CoM) distance time series, the monomer density of the single snapshot, and the pair correlation function, are quite similar to the 200-monomer case when plotted against coordinates normalized by the cylinder length. This implies that the polymers show similar behaviour across these two scales when placed under mixing constraints.

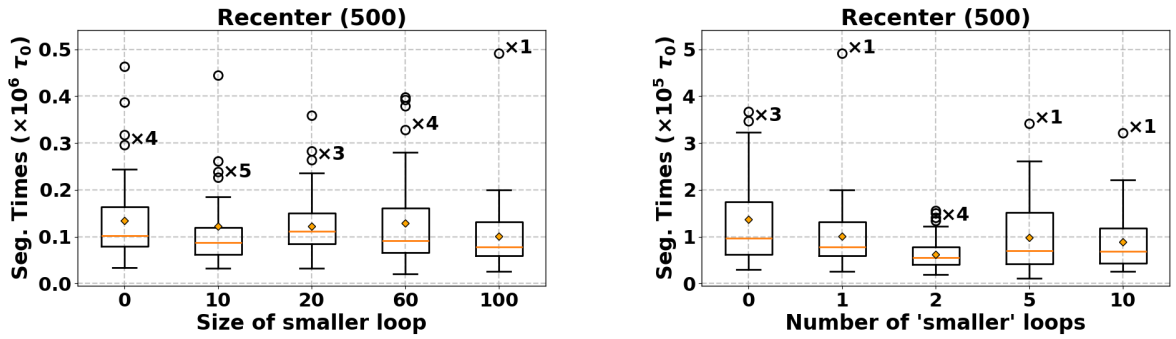

(a) (b)

Figure 3.13: The segregation box plots comparing various architectures for the *Recenter* procedure with 500 monomers in each polymer. Each box plot has an orange diamond that indicates the mean segregation time for that architecture. The numbers written close to the outliers (if any) indicate the total number of outliers for that architecture. Some outliers are not explicitly shown for clarity of the rest of the data. (a) shows the segregation times' comparison for *single-looped* topologies with varying sizes of the smaller loop (total monomers in the polymer remain constant). (b) shows the comparison for *multiple-looped* topologies with varying number of smaller loops.

3.5.2 Segregation Times

The segregation times for *single-looped* architectures and *multiple-looped* architectures are given in Figures 3.13a and 3.13b. As in the other cases, the *single-looped* architectures do not show significant differences in segregation times.

However, there is a contrast in the *multiple-looped* segregation times as compared to the 200-monomer *Recenter* case. The segregation time decreases with the number of smaller loops, as expected, but it rises again beyond Arc-1-2 (500). After some investigation, we have found that this increase in segregation time is linked to the initial orientation of the polymers in the mixed state. Of the two possibilities, antiparallel orientations lead to higher segregation times (see Figure 3.14). Arc-1-5 and Arc-1-10 polymers have a strong tendency to assume an antiparallel orientation during the mixed state due to the entropic repulsion of multiple loops. Arc-1-2 polymers, in comparison, assume a parallel orientation preferentially since the polymers are initialized like that, and the entropic repulsion between loops is low. Thus, Arc-1-5 and Arc-1-10 show higher segregation times due to a higher proportion of their mixed states being antiparallel in orientation.

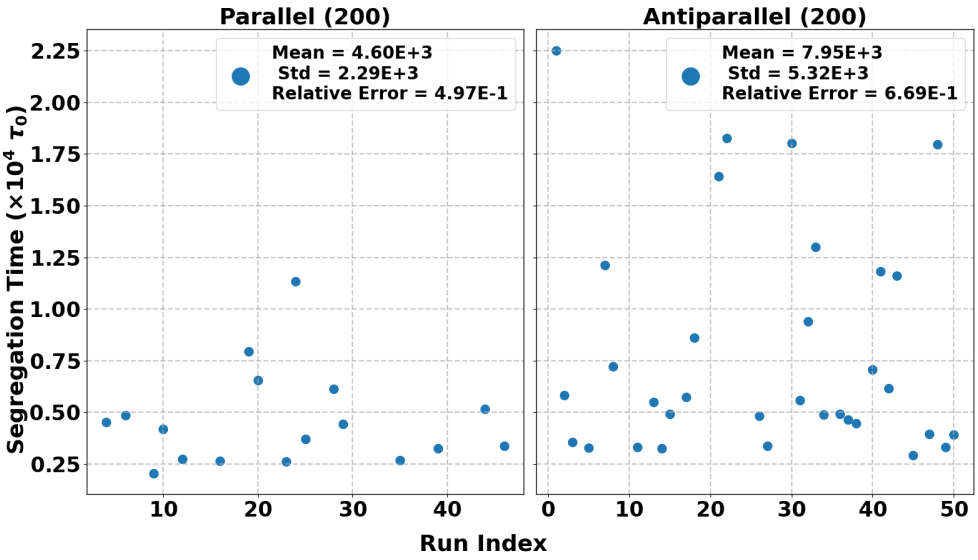

(a)

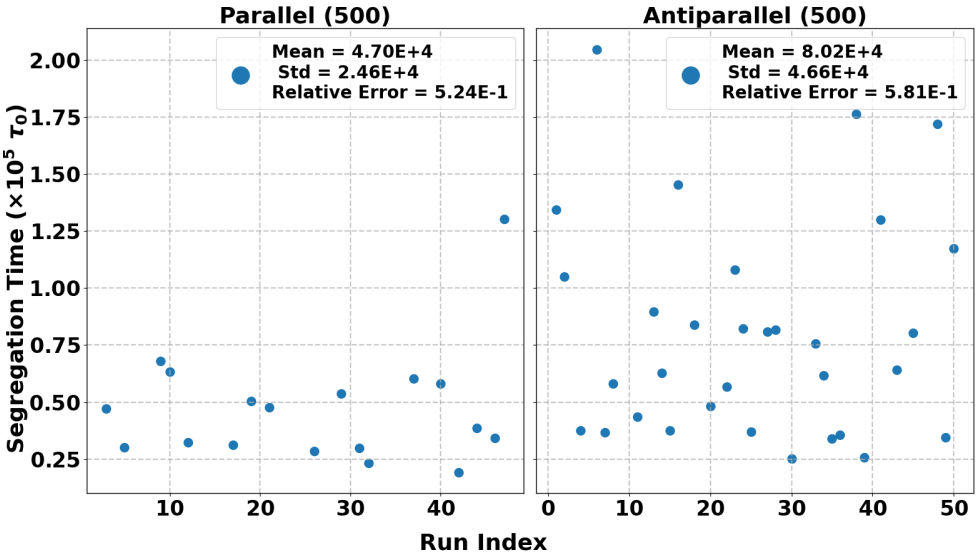

(b)

Figure 3.14: A comparison of the scatter plots of segregation times of parallel and antiparallel orientations for (a) Arc-1-5 (200) architecture and, (b) Arc-1-5 (500) architecture. The antiparallel orientations have a significantly higher mean and a higher spread than the parallel orientations in both cases. However, notice that the segregation time values for the 200-monomer case are an order of magnitude smaller than for the 500-monomer case.

We have a hypothesis as to why antiparallel polymers segregate slower, especially for polymers with multiple smaller loops. In a mixed state with antiparallel orientation, the small loops of either polymer form dense regions of monomers close to the centre of the cylinder. The two dense regions do not overlap with each other and occupy space on either side of the equatorial plane. The big loops lie close to the walls, flanking either side of the small-looped regions. The arrangement is such that the big loop of one polymer is in contact with a wall on one side and the small loops of the other polymer on the other side. For segregation to occur, the big loop regions of either polymer must diffuse across the dense small-looped region to the opposite side. This crossing involves the overlap of the big loop with the high-density small loop region, which is entropically unfavourable. Hence, the crossing poses a kinetic free energy barrier, slowing down the segregation process. We have come up with this explanation based on the visualisations of the segregation process. The initial part of the process shows stalled segregation despite no constraints being imposed, which is indicative of the presence of some free energy barrier. This observation is explained by our hypothesis; however, we have not quantified the free energy barrier.

Such an effect was observed for the case of 200 monomers as well (see Figure 3.14a). However, the segregation times of the polymers in antiparallel orientations were quite small, similar to those of the other *multiple-looped* architectures. Hence, this effect did not reveal its presence in the segregation box plots for the 200-monomer case.

In the 500-monomer case, the segregation times of antiparallel orientated polymers of *multiple-looped* architectures are comparable to that of Arc0. The higher rise in times can possibly be attributed to the slower dynamics of the bigger polymers. We cannot conclude what the exact mechanism is without studying the difference more carefully.

3.6 *Fixing-Bonding*: 500 monomers

In this section, we show the mixing and segregation data for polymers of 500 monomers each that are mixed using the *Fixing-Bonding* initialization procedure. Note that this procedure ensures the polymers are initialized in a parallel orientation.

3.6.1 Validity of mixed states

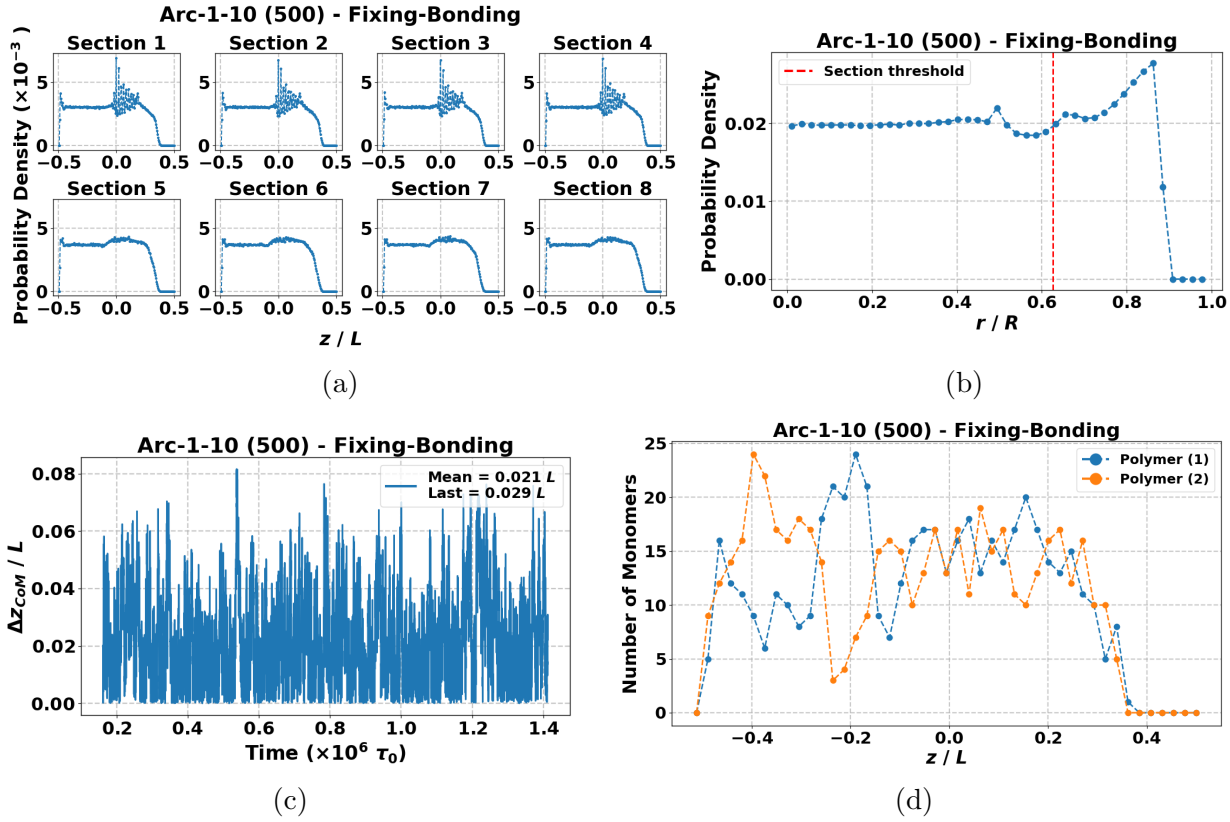

Figure 3.15: Various plots showing the monomer distribution for the mixed Arc-1-10 (500) polymers during the *Fixing-Bonding* procedure. (a) Monomer density in different sections (b) Monomer density along the radial direction (c) Time series of the distance between Polymer centres of mass (CoMs) (d) Monomer density from the mixed state snapshot. Plots (a) and (b) show how the monomers are distributed throughout the cylinder. Plots (c) and (d) show that the two polymers are well-overlapped along the long axis of the cylinder.

Figure 3.15 shows the quantities plotted to check the validity of the generated mixed states. The monomer distribution in various sections given in Figure 3.15a has the high density feature on one side of the cylinder, similar to the one seen for the 200-monomer case (see Figure 3.5a). This feature is due to the constraint of fixed particles on the equatorial plane. The radial density in Figure 3.15b shows the usual wall peak and a secondary peak indicating the position of the fixed monomers.

The centre of mass distance and single snapshot monomer distributions show that the polymers are close together and overlap well with each other.

3.6.2 Segregation Times

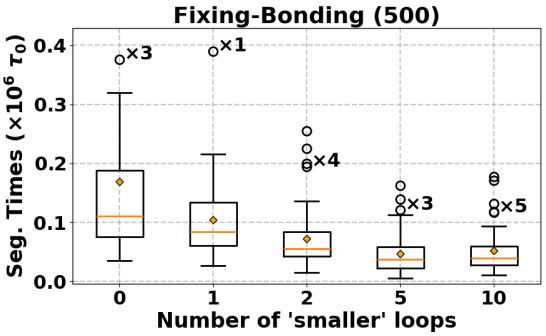

Figure 3.16: The segregation box plots comparing various architectures for the *Fixing-Bonding* procedure with 500 monomers in each polymer. The *multiple-looped* topologies with varying number of smaller loops are compared. Each box plot has an orange diamond that indicates the mean segregation time for that architecture. The numbers written close to the outliers (if any) indicate the total number of outliers for that architecture. Some outliers are not explicitly shown for clarity of the rest of the data.

For this, and the subsequent procedures, we have not plotted the segregation times to compare the *single-looped* architectures. We expect them to have very few differences among themselves, if at all. We directly consider the more interesting case of *multiple-looped* architectures as shown in Figure 3.16. In contrast to the earlier *Recenter* case, the *Fixing-Bonding* case shows the trend of decreasing segregation times as the number of loops increases. This is to be expected since the *Fixing-Bonding* initialization procedure forces all mixed states to exist in a parallel orientation. As explained in Section 3.5.2, *multiple-looped* polymers in a parallel orientation segregate faster without the need to cross a kinetic barrier. Hence, the segregation times' means are small in the present case as compared to the *Recenter* case.

3.7 *Replication-like*: 500 monomers

Here, we show the data obtained for polymers having 500 monomers initialized using the *Replication-like* procedure. Again, this procedure ensures the polymers are initialized in a parallel orientation.

3.7.1 Validity of mixed states

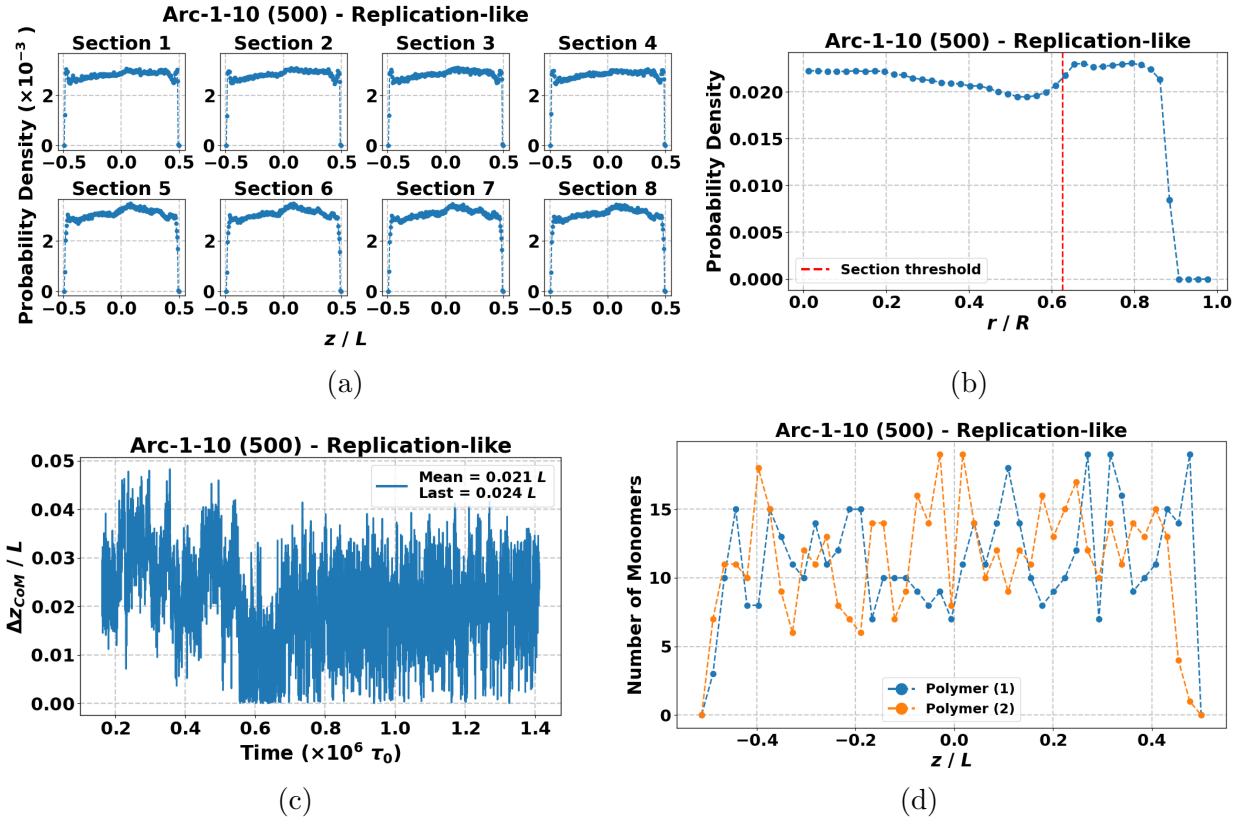

Figure 3.17: Various plots showing the monomer distribution for the mixed Arc-1-10 (500) polymers during the *Replication-like* procedure. (a) Monomer density in different sections (b) Monomer density along the radial direction (c) Time series of the distance between Polymer centres of mass (CoMs) (d) Monomer density from the mixed state snapshot. Plots (a) and (b) show how the monomers are distributed throughout the cylinder. Plots (c) and (d) show that the two polymers are well-overlapped along the long axis of the cylinder.

We again plot the quantities as shown in Figure 3.17 to validate the mixed state for this procedure. The sectional monomer density in Figure 3.17a is similar to the 200-monomer case but the density is more uniform. A slight asymmetry still exists. The radial density in Figure 3.17b clearly shows the wall effect. However, the interpolymer bonds do not seem to affect the radial density in the 500-monomer case. The radial dednsity is similar to the one plotted for the *Recenter* (500) procedure.

As we have seen multipe times so far, the centre of mass distance and single snapshot monomer density indicate that the polymers are mixed well.

3.7.2 Segregation Times

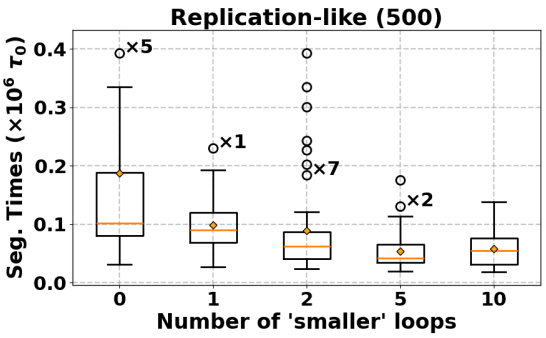

Figure 3.18: The segregation box plots comparing various architectures for the *Replication-like* procedure with 500 monomers in each polymer. The *multiple-looped* topologies with varying number of smaller loops are compared. Each box plot has an orange diamond that indicates the mean segregation time for that architecture. The numbers written close to the outliers (if any) indicate the total number of outliers for that architecture. Some outliers are not explicitly shown for clarity of the rest of the data.

We compare the segregation times of various *multiple-looped* architectures in Figure 3.18. Again, we see that the segregation times' mean and spread decrease as the number of loops increase beyond one. Such a trend is expected since all mixed states have polymers in a parallel orientation, which is consistent with the *Fixing-Bonding* case as well.

3.8 *Mutual Attraction*: 500 monomers

Finally, we present the data for 500-monomer polymers mixed using the *Mutual Attraction* initialization procedure.

3.8.1 Validity of Mixed States

We plot the usual quantities to check for the validity of the mixed states in Figure 3.19. The sectional monomer density in figure 3.19a dips close to the end cap walls as expected for the *Mutual Attraction* procedure. However, there is an additional slight dip at the centre of the cylinder in all sections. This dip separates the two regions of relatively higher density on

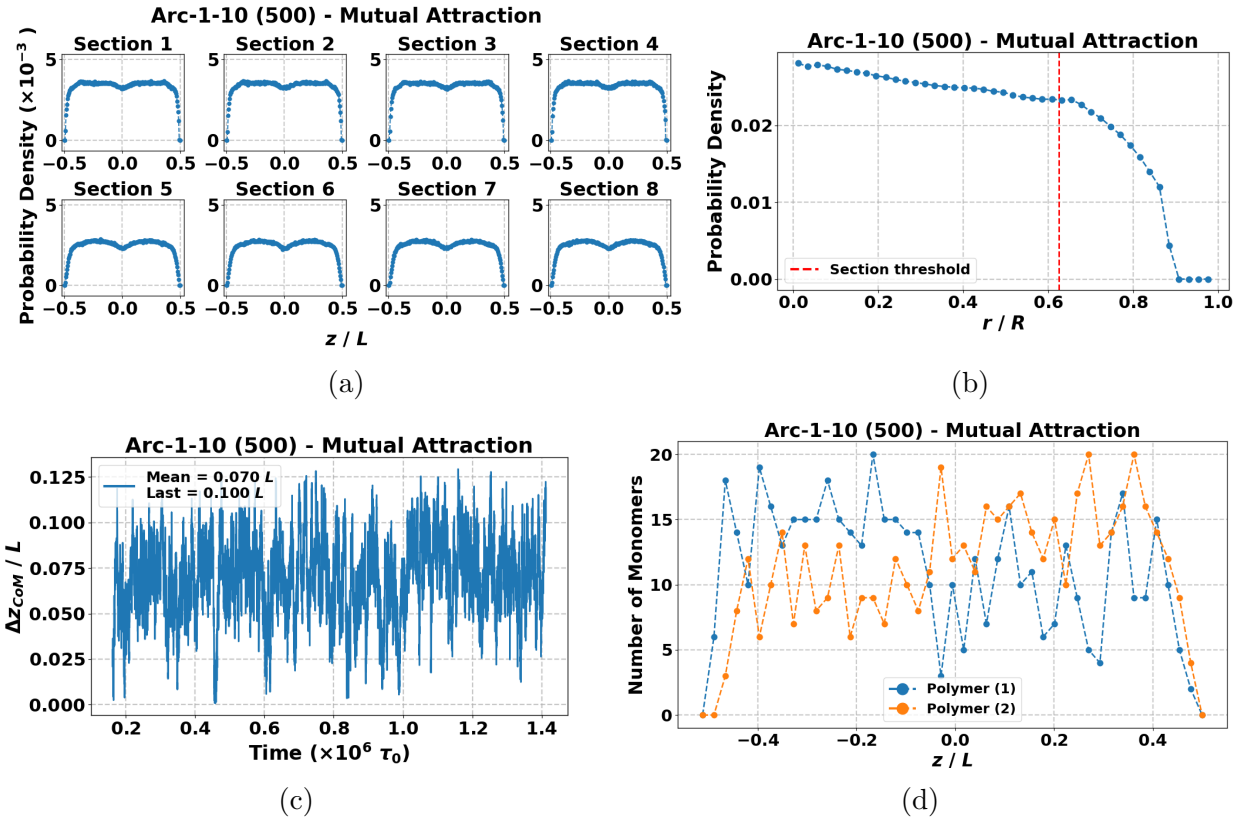

Figure 3.19: Various plots showing the monomer distribution for the mixed Arc-1-10 (500) polymers during the *Mutual Attraction* procedure. (a) Monomer density in different sections (b) Monomer density along the radial direction (c) Time series of the distance between Polymer centres of mass (CoMs) (d) Monomer density from the mixed state snapshot. Plots (a) and (b) show how the monomers are distributed throughout the cylinder. Plots (c) and (d) show that the two polymers are well-overlapped along the long axis of the cylinder.

either side. Our guess is that the multiple small loops of an Arc-1-10 (500) polymer forms a dense compact region on one side of the cylinder which attracts the monomers from the other polymer too. This same thing happens for the small loops of the other polymer on the other side of the cylinder. These two desne regions repel each other entropically, leaving a slight gap in the middle. The radial density in Figure 3.19b highlights the lack of the wall effect as a consequence of the attraction between monomers.

Figures 3.19c shows the time series of the centre of mass distance. Although the centre of mass distance is high compared to other procedures, it stays below $0.15L$ at all times. The monomer density of the last snapshot (Figure 3.19d) shows that the polymers are well overlapped despite the distance between their centres of mass.

3.8.2 Segregation Times

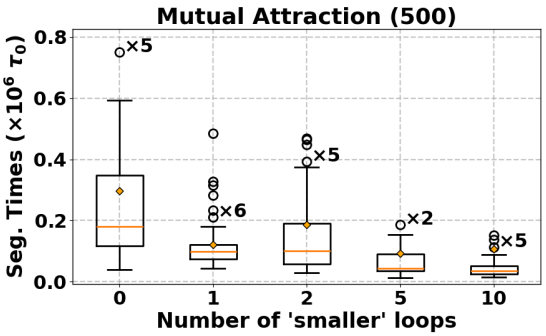

Figure 3.20: The segregation box plots comparing various architectures for the *Mutual Attraction* procedure with 500 monomers in each polymer. The *multiple-looped* topologies with varying number of smaller loops are compared. Each box plot has an orange diamond that indicates the mean segregation time for that architecture. The numbers written close to the outliers (if any) indicate the total number of outliers for that architecture. Some outliers are not explicitly shown for clarity of the rest of the data.

In Figure 3.20, we show the segregation times of different *multiple-looped* architectures. The trend is similar to the 200-monomer *Mutual Attraction* case discussed in Section 3.4.2. The segregation times' means and spreads decrease with increasing number of loops, but Arc1-2 defies the general trend. The high segregation times for the Arc1-2 case can be attributed to the threading effect explained in Section 3.4.2, which affects Arc1-2 disproportionately as compared to other architectures.

The segregation data for *Recenter* (500) and *Mutual Attraction* (500) shows that the initialization procedure can affect the segregation trends of the architectures. There exists a general trend of decreasing segregation times as the number of loops increases, but it is sensitive to the initialization procedure.

3.9 Statistical Tests

Finally, we give a few examples of the statistical tests we performed on our obtained data as described in Section 2.7. Using the *two-tailed t-test*, we calculate the *p-value* for each pair of architecture for one particular initialization procedure. A *p-value* is the probability that

	Arc0	Arc-1-1	Arc-1-2	Arc-1-5	Arc-1-10
Arc0		0.3389	0.0532	0.0159	0.0102
Arc-1-1			0.0056	< 0.0001	< 0.0001
Arc-1-2				0.1997	0.0659
Arc-1-5					0.4559

Table 3.1: The *p-values* for the segregation times of various architectures initialized using the *Recenter* procedure. This is for the case of polymers with 200 monomers each. Each *p-value* gives the probability that the two architectures it represents is statistically identical. The cells highlighted in light green have the *p-values* below the significance threshold $\alpha = 0.05$ which means that the times of the architectures are significantly different.

	Arc0	Arc-1-1	Arc-1-2	Arc-1-5	Arc-1-10
Arc0		0.0675	< 0.0001	0.0522	0.0094
Arc-1-1			0.0009	0.8296	0.3245
Arc-1-2				0.0043	0.0091
Arc-1-5					0.4834

Table 3.2: The *p-values* for the segregation times of various architectures initialized using the *Recenter* procedure. This is for the case of polymers with 500 monomers each. Each *p-value* gives the probability that the two architectures it represents is statistically identical. The cells highlighted in light green have the *p-values* below the significance threshold $\alpha = 0.05$ which means that the times of the architectures are significantly different.

the segregation times of the two architectures being compared are statistically identical. We consider the difference between two architectures to be statistically significant if the *p-value* is below the significance value of $\alpha = 0.05$.

The *p-values* are presented in tables as shown in Tables 3.1 and 3.2. The value mentioned at the location of column ArcX and row ArcY is the *p-value* comparing ArcX and ArcY. Only the upper diagonal part of the table is filled since the order of the architectures does not matter while comparing. Comparisons between the same architecture would yield a *p-value* of 1 by definition, and are not shown for clarity.

Table 3.1 shows the *p-values* for the *multiple-looped* architectures initialized using the *Recenter* procedure on 200-momomer polymers. We can infer that segregation times of Arc-1-1 are significantly different than those of the *multiple-looped* architectures. The same can be said for Arc0, except for the comparison between Arc0 and Arc-1-2, whose *p-value* is just above the threshold.

We have shown the *p-values* for the corresponding 500-monomer case in Table 3.2. In contrast to the 200-monomer case, here the *p-values* show a different trend. Arc-1-2 is significantly distinct when compared to any other *multiple-looped* architecture. However, Arc-1-5 and Arc-1-10 have higher segregation times as compared to Arc-1-2 such that they are not distinguishable from Arc-1-1. These results reflect what we observed by plotting the box plots of the segregation times.

In summary, such a statistical test that quantify the differences between the segregation times of various architectures. We find that in a majority of the cases, the architectures with higher number of loops show a statistically distinct distribution of segregation times compared to *single-looped* architectures.

Chapter 4

Discussion

In this work, we have characterised the segregation times of various polymers in cylindrical confinement. We considered segregation between non-concatenated identical polymers having topological modifications in the form of loops. In order to find the segregation time, we introduced multiple independent procedures to create mixed states of the polymers such that they remain non-concatenated. As explained earlier (Section 2.3), obtaining such mixed states in a confined cylinder has not been a trivial task. However, we managed to obtain mixed states by imposing certain constraints on the polymer system.

Once we had valid mixed states, we let the two polymers segregate by removing the constraints. Once the constraints were lifted, the segregation occurred spontaneously. This is because the polymers can achieve a greater number of conformations in the segregated state than in the mixed state. The increase in entropy drives the segregation of polymers in confinement.

In order to establish beyond doubt that the segregation is indeed an entropic effect, we plotted the system energy during segregation as a function of time. The trajectory starts with the polymers in a mixed state and ends with the segregated state. Figure 4.1 shows the different components of the system's total energy (normalised by the number of monomers). As can be seen in the plot, all components of energy remain roughly the same throughout the simulation. Crucially, the energy of the system does not change when going from the mixed to the segregated state. Since we observe the segregation to be spontaneous, the Helmholtz free energy F must be decreasing. If the energy (or enthalpy) is constant, then, by virtue

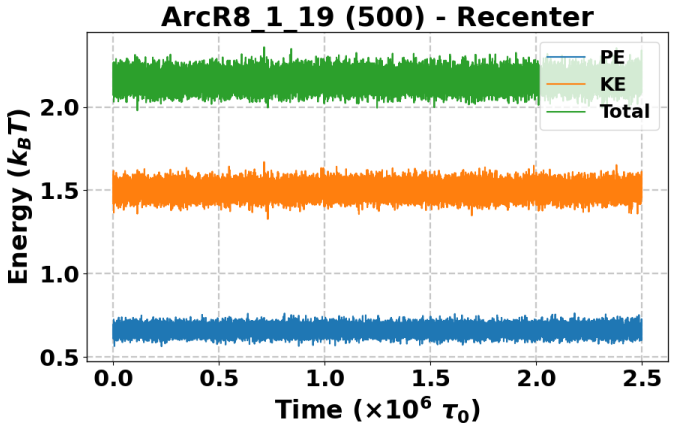

Figure 4.1: The system energy per monomer plotted as a function of time. It shows the kinetic energy (KE) component, the potential energy (PE) component, and the total energy. The energy stays roughly constant over the entire segregation run. This run is the same run that was plotted for the segregation trajectory in Figure 2.6

of Equation 1.1, the entropy must increase to decrease the free energy. Thus, the polymers prefer to stay segregated rather than overlapped in confinement due to entropic reasons.

In this study, we consider different topologies and investigate the entropic effect. For the *single-looped* architectures (architectures with one subloop in addition to the ring), we see no segregation speed up as compared to the ring polymer. Additionally, there is no speed-up even when we change the size of the subloops while keeping the total size of the polymer constant. These results agree with the free energy calculations introduced in the previous work [18] where it was shown that there is no gain in the free energy difference for *single-looped* architectures. Further, We systematically varied the number of subloops in *multiple-looped* architectures and found an almost universal trend. As the number of subloops increases, the segregation becomes faster. Again, this is in line with the results of the previous study [18].

There were two exceptions to the trend stated above. One of the initialization procedures, *Mutual Attraction*, favoured the entanglements of the two polymers in the cylinder, further slowing down segregation. The degree of entanglement was different for different architectures; thus, they added an additional factor affecting the time of segregation. As a result, Arc-1-2 showed the highest segregation time, in contrast to mixed states generated by other procedures. The other exception occurred in the case of polymers with 500 monomers mixed using the *Recenter* procedure. In this bigger system, we expected the entropic forces

to be enhanced and to obtain starker differences in segregation times across architectures. However, we found that Arc-1-5 and Arc-1-10 showed higher segregation times than Arc-1-2. The increase in the segregation times could be attributed to another factor affecting segregation: the initial orientation of the two polymers. Arc-1-5 and Arc-1-10 have a greater tendency to occur in the antiparallel orientation, which is found to segregate slower than polymers in parallel orientation. Hence, Arc-1-5 and Arc-1-10 show slower segregation.

Despite our expectations, the segregation time is not solely dependent on number of loops in the polymer topology. But these results are still relevant in the case of rod-shaped bacterial cells, which are known to form loops [16, 17] on the chromatin. We expect such loops to play a role in achieving timely segregation of the chromosome. There might be other conditions within a cell that can make this segregation more robust than synthetic polymers in confinement. Such conditions could be investigated in future work. Apart from the biological context, we also expect such segregation properties of polymers to be useful for industrial applications. Polymers could be manufactured with topological modifications to tune their properties irrespective of their chemical composition. However, this study considered many simplifying assumptions and should only be taken as a starting point. It should be verified that these results remain unchanged when other experimentally relevant conditions (for example, hydrodynamics effects) are introduced in the simulations.

In this vein, there are multiple other ways this work can be taken forward. We have studied the segregation times for polymers containing 200 and 500 monomers each. In addition, the segregation can be studied for even bigger polymers with the aim of establishing a scaling relation between the segregation time and size N.

In this study, we kept the cylinder diameter constant while varying the topology. However, adding cross-links can change the natural size of the polymers, and each topology may feel a different degree of confinement as a result. Thus, it might be useful to vary the diameter of the cylinder to keep its ratio with the polymer's natural size constant. Such a study would investigate the segregation time while keeping the degree of confinement constant, unlike the present study.

Complementary to the work done in this thesis, one could investigate the effect on segregation times if one allows chain crossing to occur. In bacterial cells, certain proteins exist that can cause two DNA strands to pass through one another. Thus, such a study would be more relevant to a biological context.

Bibliography

[1]A. M. Menzel, "Tuned, driven, and active soft matter", Physics Reports, Tuned, driven, and active soft matter **554**, 1–45 (2015).

[2]P.-G. de Gennes, "Soft matter (nobel lecture)", Angewandte Chemie International Edition in English **31**, _eprint: https://onlinelibrary.wiley.com/doi/pdf/10.1002/anie.199208421, 842–845 (1992).

[3]R. Jones, *Soft condensed matter*, Oxford Master Series in Physics (OUP Oxford, 2002).

[4]M. Doi, *Soft matter physics* (OUP Oxford, 2013).

[5]*Soft matter physics — institute of physics*, https://www.iop.org/explore-physics/big-ideas-physics/soft-matter-physics (visited on 02/14/2025).

[6]D. Feldman, "Polymer history", Designed Monomers and Polymers **11**, 1–15 (2008).

[7]E. A. Hauser, "The historical background of colloid chemistry", Journal of Chemical Education **27**, Publisher: American Chemical Society, 264 (1950).

[8]D. A. Weitz, "Soft materials evolution and revolution", Nature Materials **21**, Publisher: Nature Publishing Group, 986–988 (2022).

[9]T. McLeish, "Soft matter – an emergent interdisciplinary science of emergent entities", in *The routledge handbook of emergence*, Num Pages: 17 (Routledge, 2019).

[10]M. Rubinstein and R. Colby, *Polymer physics* (Oxford University Press, 2003).

[11]A. Santra and J. Ravi Prakash, "Universality of dilute solutions of ring polymers in the thermal crossover region between and athermal solvents", Journal of Rheology **66**, 775–792 (2022).

[12]L. Tubiana, G. P. Alexander, A. Barbensi, D. Buck, J. H. E. Cartwright, M. Chwastyk, M. Cieplak, I. Coluzza, S. Čopar, D. J. Craik, M. Di Stefano, R. Everaers, P. F. N. Faísca, F. Ferrari, A. Giacometti, D. Goundaroulis, E. Haglund, Y.-M. Hou, N. Ilieva, S. E. Jackson, A. Japaridze, N. Kaplan, A. R. Klotz, H. Li, C. N. Likos, E. Locatelli, T. López-León, T. Machon, C. Micheletti, D. Michieletto, A. Niemi, W. Niemyska, S. Niewieczerzal, F. Nitti, E. Orlandini, S. Pasquali, A. P. Perlinska, R. Podgornik, R. Potestio, N. M. Pugno, M. Ravnik, R. Ricca, C. M. Rohwer, A. Rosa, J. Smrek, A. Souslov, A. Stasiak, D. Steer, J. Sułkowska, P. Sułkowski, D. W. L. Sumners, C. Svaneborg, P. Szymczak, T. Tarenzi, R. Travasso, P. Virnau, D. Vlassopoulos, P. Ziherl, and S. Žumer, "Topology in soft and biological matter", Physics Reports, Topology in soft and biological matter **1075**, 1–137 (2024).

[13]T. McLeish, "Polymers without beginning or end", Science **297**, Publisher: American Association for the Advancement of Science, 2005–2006 (2002).

[14]J. D. Halverson, J. Smrek, K. Kremer, and A. Y. Grosberg, "From a melt of rings to chromosome territories: the role of topological constraints in genome folding", Reports on Progress in Physics **77**, Publisher: IOP Publishing, 022601 (2014).

[15]C. Micheletti, D. Marenduzzo, and E. Orlandini, "Polymers with spatial or topological constraints: theoretical and computational results", Physics Reports **504**, 1–73 (2011).

[16]M. Ganji, I. A. Shaltiel, S. Bisht, E. Kim, A. Kalichava, C. H. Haering, and C. Dekker, "Real-time imaging of DNA loop extrusion by condensin", Science **360**, Publisher: American Association for the Advancement of Science, 102–105 (2018).

[17]S. Kadauke and G. A. Blobel, "Chromatin loops in gene regulation", Biochimica et Biophysica Acta (BBA) - Gene Regulatory Mechanisms, Epigenetics **1789**, 17–25 (2009).

[18]D. Mitra, S. Pande, and A. Chatterji, "Topology-driven spatial organization of ring polymers under confinement", Physical Review E **106**, Publisher: American Physical Society, 054502 (2022).

[19]K. Roychoudhury, S. Pande, I. S. Shashank, D. Mitra, and A. Chatterji, *Entropic organization of topologically modified ring polymers in spherical confinement*, Jan. 4, 2025.

[20]D. Mitra, S. Pande, and A. Chatterji, "Polymer architecture orchestrates the segregation and spatial organization of replicating e. coli chromosomes in slow growth", Soft Matter **18**, Publisher: The Royal Society of Chemistry, 5615–5631 (2022).

[21]S. Pande, D. Mitra, and A. Chatterji, "Topology-mediated organization of escherichia coli chromosome in fast-growth conditions", Physical Review E **110**, Publisher: American Physical Society, 054401 (2024).

[22]A. Y. Grosberg, P. G. Khalatur, and A. R. Khokhlov, "Polymeric coils with excluded volume in dilute solution: the invalidity of the model of impenetrable spheres and the influence of excluded volume on the rates of diffusion-controlled intermacromolecular reactions", Die Makromolekulare Chemie, Rapid Communications **3**, _eprint: https://onlinelibrary.wiley.com/doi/pdf/10. 709–713 (1982).

[23]S. Jun and B. Mulder, "Entropy-driven spatial organization of highly confined polymers: lessons for the bacterial chromosome", Proceedings of the National Academy of Sciences **103**, Publisher: Proceedings of the National Academy of Sciences, 12388–12393 (2006).

[24]J. M. Polson and L. G. Montgomery, "Polymer segregation under confinement: free energy calculations and segregation dynamics simulations", The Journal of Chemical Physics **141**, 164902 (2014).

[25]Y. Jung and B.-Y. Ha, "Overlapping two self-avoiding polymers in a closed cylindrical pore: implications for chromosome segregation in a bacterial cell", Physical Review E **82**, Publisher: American Physical Society, 051926 (2010).

[26]S. Jun and A. Wright, "Entropy as the driver of chromosome segregation", Nature Reviews Microbiology **8**, Publisher: Nature Publishing Group, 600–607 (2010).

[27]D. Marenduzzo, "The physics of DNA and chromosomes", in *The physics of DNA and chromosomes* (IOP Publishing, Oct. 1, 2018).

[28]Y. Chen, W. Yu, J. Wang, and K. Luo, "Polymer segregation under confinement: influences of macromolecular crowding and the interaction between the polymer and crowders", The Journal of Chemical Physics **143**, 134904 (2015).

[29]A. Narros, A. J. Moreno, and C. N. Likos, "Influence of topology on effective potentials: coarse-graining ring polymers", Soft Matter **6**, Publisher: Royal Society of Chemistry, 2435–2441 (2010).

[30]A. Narros, C. N. Likos, A. J. Moreno, and B. Capone, "Multi-blob coarse graining for ring polymer solutions", Soft Matter **10**, 9601–9614 (2014).

[31]K. Kremer and G. S. Grest, "Dynamics of entangled linear polymer melts: a molecular-dynamics simulation", The Journal of Chemical Physics **92**, 5057–5086 (1990).

[32]J. D. Weeks, D. Chandler, and H. C. Andersen, "Role of repulsive forces in determining the equilibrium structure of simple liquids", The Journal of Chemical Physics **54**, 5237–5247 (1971).

[33]A. P. Thompson, H. M. Aktulga, R. Berger, D. S. Bolintineanu, W. M. Brown, P. S. Crozier, P. J. in 't Veld, A. Kohlmeyer, S. G. Moore, T. D. Nguyen, R. Shan, M. J. Stevens, J. Tranchida, C. Trott, and S. J. Plimpton, "LAMMPS - a flexible simulation tool for particle-based materials modeling at the atomic, meso, and continuum scales", Comp. Phys. Comm. **271**, 108171 (2022).

[34]M. Çetinkaya-Rundel and J. Hardin, *Introduction to modern statistics*, Open Library ID: OL52653361M (OpenIntro, Inc., 2024).

[35]D. Frenkel and B. Smit, *Understanding molecular simulation: from algorithms to applications*, Google-Books-ID: 5qTzldS9ROIC (Elsevier, Oct. 19, 2001), 661 pp.

[36]A. Stukowski, "Visualization and analysis of atomistic simulation data with ovito–the open visualization tool", Modelling and Simulation in Materials Science and Engineering **18**, 015012 (2009).